



More than the clock: distinct regulation of muscle function and metabolism by PER2 and ROR α

Shivani Mansingh¹ , Geraldine Maier¹, Julien Delezie¹, Pål O. Westermark², Danilo Ritz¹, Wandrille Duchemin³, Gesa Santos¹, Bettina Karrer-Cardel¹, Stefan A. Steurer¹, Urs Albrecht⁴  and Christoph Handschin¹ 

¹Biozentrum, University of Basel, Basel, Switzerland

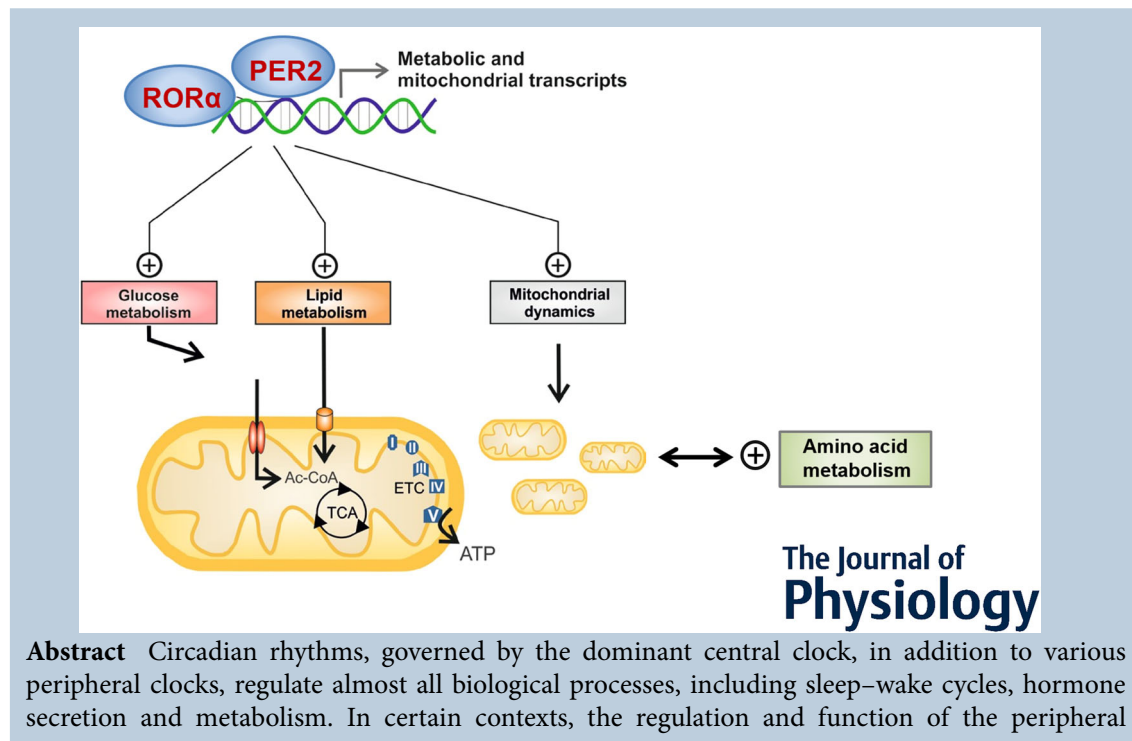
²Leibniz-Institut für Nutztierbiologie, Institut für Genetik und Biometrie, Dummerstorf, Germany

³sciCORE Center for Scientific Computing, University of Basel, Basel, Switzerland

⁴Department of Biology, University of Fribourg, Fribourg, Switzerland

Handling Editors: Paul Greenhaff & Josiane Broussard

The peer review history is available in the Supporting Information section of this article (<https://doi.org/10.1113/JP285585#support-information-section>).



Shivani Mansingh is currently pursuing her PhD in Molecular Biology at the Biozentrum, University of Basel. She is interested in exercise, circadian biology and neuroscience, with a particular focus on how neuromuscular signalling is affected by physiological factors, such as circadian rhythms and exercise. **Geraldine Maier** earned her PhD in Biomedical Research in 2020 at the Biozentrum, University of Basel. Currently, she is a postdoctoral researcher in the Wu Tsai Human Performance Alliance at the Salk Institute for Biological Studies in San Diego. Geraldine's research contributes to interdisciplinary efforts to understand and enhance human performance.



S. Mansingh and G. Maier contributed equally to this work.

oscillations can be decoupled from the central clock. However, the specific mechanisms underlying muscle-intrinsic clock-dependent modulation of muscle function and metabolism remain unclear. We investigated the outcome of perturbations of the primary and secondary feedback loops of the molecular clock in skeletal muscle by specific gene ablation of Period circadian regulator 2 (*Per2*) and RAR-related orphan receptor alpha (*Rora*), respectively. In both models, a dampening of core clock gene oscillation was observed, while the phase was preserved. Moreover, both loops seem to be involved in the homeostasis of amine groups. Highly divergent outcomes were seen for overall muscle gene expression, primarily affecting circadian rhythmicity in the *PER2* knockouts and non-oscillating genes in the *ROR α* knockouts, leading to distinct outcomes in terms of metabolome and phenotype. These results highlight the entanglement of the molecular clock and muscle plasticity and allude to specific functions of different clock components, i.e. the primary and secondary feedback loops, in this context. The reciprocal interaction between muscle contractility and circadian clocks might therefore be instrumental to determining a finely tuned adaptation of muscle tissue to perturbations in health and disease.

(Received 28 August 2023; accepted after revision 20 May 2024; first published online 8 June 2024)

Corresponding author C. Handschin: University of Basel, Biozentrum, Basel, Switzerland. Email: christoph.handschin@unibas.ch

Abstract figure legend This study evaluates the functional and molecular consequences of modulating different regulatory loops of the muscle-intrinsic clock, through extensive phenotypic, transcriptomic, proteomic and metabolomic profiling of the muscle around the clock. Overall, deletion of *PER2* and *ROR α* and, as a proxy, modulation of the primary or secondary feedback arms, leads to shared but distinct outcomes in terms of the transcriptome, proteome and phenotype. Perturbations of both the primary (*PER2* MKO) and secondary arms (*ROR α* MKO) of the core clock dampen the amplitude of expression of many clock and clock-associated genes but do not affect their phase, thereby maintaining basic circadian oscillation in the muscle. The deletion of *PER2* and *ROR α* affects muscle metabolism and homeostasis in a circadian manner, through modulation of metabolic and mitochondrial genes, which encode proteins involved in amino acid metabolism, the tricarboxylic acid (TCA) cycle and mitochondrial biogenesis, thereby affecting amino acid and ion homeostasis. As a result, glucose and lipid metabolism, in addition to amino acid metabolism, are impacted in these knockouts, highlighting the central role of the molecular clock in modulating muscle plasticity. ATP: adenosine triphosphate, ETC: electron transport chain.

Key points

- Specific perturbations of the primary and secondary feedback loop of the molecular clock result in specific outcomes on muscle metabolism and function.
- Ablation of *Per2* (primary loop) or *Rora* (secondary loop) blunts the amplitude of core clock genes, in absence of a shift in phase.
- Perturbation of the primary feedback loop by deletion of *PER2* primarily affects muscle gene oscillation.
- Knockout of *ROR α* and the ensuing modulation of the secondary loop results in the aberrant expression of a large number of non-clock genes and proteins.
- The deletion of *PER2* and *ROR α* affects muscle metabolism and contractile function in a circadian manner, highlighting the central role of the molecular clock in modulating muscle plasticity.

Introduction

The circadian system, driven by an internal biological clock, intricately regulates a multitude of physiological functions, encompassing sleep–wake patterns, hormonal release and metabolic processes (Bass & Lazar, 2016). The suprachiasmatic nucleus within

the hypothalamus governs the central pacemaker, dictating the master circadian rhythm (Takahashi et al., 2008), while endogenous clocks within various tissues, forming what is known as peripheral clock networks, provide an additional level of control (Eckel-Mahan & Sassone-Corsi, 2013). Period circadian regulator 2 (*PER2*) and RAR-related orphan receptor alpha (*ROR α*) are major

components of the circadian clock pathway, with PER2 forming the primary, core feedback loop and ROR α modulating the secondary feedback arm. PER exhibits peak activity at the beginning of the active phase (daytime in humans or night-time in mice) and forms repressor complexes with cryptochrome circadian regulator (CRY) that inhibit transcriptional activity of clock circadian regulator (CLOCK) and basic helix-loop-helix ARNT Like 1 (BMAL1), thus, in turn, repressing their own transcription (Bass & Takahashi, 2010; Partch et al., 2014). The secondary arm of the loop is composed of the orphan nuclear receptors retinoic acid-related orphan receptors (ROR $\alpha/\beta/\gamma$, NR1F1) and nuclear receptor subfamily 1 group D members (REV-ERB α/β , NR1D1/2), which exert opposite effects on the molecular clock by activating or repressing BMAL1 transcription, respectively, via ROR response element (RORE) transcription sequences located within the BMAL1 promoter (Partch et al., 2014; Takahashi, 2017). Not only can these factors generate tissue-specific circadian outputs by interacting with tissue-specific transcription factors, but they can also regulate the expression of hundreds of genes outside the circadian feedback loop, in a highly tissue-specific manner, and thereby connect circadian rhythms functionally to physiological adaptations (Dibner et al., 2010).

Owing to the increased metabolic disorders observed in individuals with desynchronized circadian rhythms, the skeletal muscle clock has emerged as an interesting candidate for understanding how tissue-specific clock function and (patho)physiology are linked (Gutierrez-Monreal et al., 2020; Mansingh & Handschin, 2022; Marcheiva et al., 2010; Martin et al., 2023a). The circadian clock within skeletal muscle governs a rhythmic pattern of gene expression that influences critical physiological processes integral to muscle function and metabolism (Dyar et al., 2014; Gutierrez-Monreal et al., 2020; Mansingh & Handschin, 2022; Zamboni et al., 2003). These circadian changes in gene expression are achieved through signalling pathways involving the CLOCK/BMAL1 complex, PER and CRY proteins and act as a regulatory mechanism to optimize muscle performance in synchrony with the daily light–dark cycle (Dibner et al., 2010; Martin et al., 2023a; Zamboni et al., 2003). The *Per* genes are important elements of these transcriptional/translational feedback loops and have been studied in various cell types as a readout for functional endogenous circadian rhythms. Global *Per2* deletion *in vitro* or *in vivo* results in diminished circadian gene expression (Zheng et al., 2001), shortened clock period lengths (Pendergast et al., 2010), reduced locomotor activity in mice (Bae et al., 2006, 2001) and impaired muscle regeneration (Katoku-Kikyo et al., 2021). ROR α knockout (KO) mice exhibit dyslipidaemia, aberrant feeding and locomotion, muscle atrophy and

ataxia in some models, such as the ROR $\alpha^{sg/sg}$ mice (Steinmayr et al., 1998), while displaying improved metabolic function and reduced inflammation in other models, such as the E11aROR α KOs (Billon et al., 2017). However, it remains unclear whether the clock components exert the muscle phenotypes in their capacity as clock genes, via non-clock biological functions in the muscle, or indirectly, by affecting other tissues. Muscle-specific consequences of CLOCK and BMAL1 deletion have been described extensively, including impaired glucose metabolism, insulin resistance and myogenesis, and indicate that ablation of the core clock significantly alters muscle metabolism (Andrews et al., 2010; Dyar et al., 2018; Harfmann et al., 2016; Peek et al., 2017; Perrin et al., 2018). However, it is unclear how potentially more subtle perturbations of the primary and secondary feedback loops impinge on the function of the skeletal muscle. Muscle-specific deletion of *Per1* and *Per2* result in suppressed myoblast differentiation *in vitro* and reduced muscle regeneration *in vivo* (Katoku-Kikyo et al., 2021), whereas repression of *Rora*, both *in vitro* and *in vivo*, leads to dysregulated metabolism, in the form of altered insulin signalling and glucose tolerance in the muscle (Raichur et al., 2010). An important point to note here is that given that *Rora* is an upstream regulator of *Bmal1*, repression of *Rora* also leads to the downregulation of *Bmal1*. As a consequence, the muscle phenotype in the ROR α KO mice could be expected to be similar to that of the BMAL1 KO, which is reflected in the shared impairments in glucose metabolism and insulin resistance in the two KO models. In light of the proposed effects of PER2 and ROR α on pathways that are not directly linked to the core clock (Katoku-Kikyo et al., 2021; Raichur et al., 2010), the functional consequences of these transcriptional regulators require deeper exploration, especially in the context of secondary gene networks. Specifically, how these factors align with muscle function, energy metabolism and performance throughout the day–night cycle and, potentially, in a non-oscillating manner, remains to be deciphered. Lastly, we are also missing a comprehensive understanding of the temporal orchestration of gene expression patterns in the skeletal muscle over the 24 h cycle in response to muscle-specific ablation of circadian factors.

To address these gaps in knowledge, in this study we looked at how perturbations of the primary and secondary loops of the muscle-intrinsic clock, by targeting PER2 and ROR α , respectively, affect whole-body physiology, in addition to skeletal muscle-specific function muscle, over the 24 h circadian cycle. To do this, we generated muscle-specific KO lines for PER2 and ROR α and performed extensive physiological, transcriptomic, proteomic and metabolomic characterization of these lines around the clock.

Methods

Ethics approval

All experiments were performed in accordance with the principles of the Basel Declaration and with Federal and Cantonal Laws regulating the care and use of experimental animals in Switzerland, in addition to institutional guidelines of the Biozentrum and the University of Basel. The protocol, with all methods described here, was approved by the 'Kantonales Veterinäramt' of the Kanton Basel-Stadt (licence numbers 2329 and 3110), under consideration of the well-being of the animals and the 3R principle. Animals chosen for the studies were randomized, and experiments were performed in a blinded manner wherever possible.

Animals

A skeletal muscle-specific KO of Period 2 (PER2 MKO) was created by crossing mice with floxed *Per2* alleles (*Per2*^{fllox/fllox}; Chavan et al., 2016) with HSA-Cre transgenic mice (purchased from the Jackson Laboratory; stock no. 006149). A skeletal muscle-specific KO of retinoid-related orphan receptor alpha (ROR α MKO) was created by crossing mice with floxed *Rora* alleles (*Rora*^{fllox/fllox}; Mouse Clinical Institute, Strasbourg, France) with HSA-Cre transgenic mice (purchased from the Jackson Laboratory; stock no. 006149). All mice were maintained on a C57BL/6J genetic background in the animal facility of the Biozentrum (University of Basel) under a 12 h–12 h light–dark cycle (lights on at 06.00 h). Unless specifically mentioned, all experiments were performed in young adult male mice (3–6 months old) housed in standard cages with bedding substrates that had *ad libitum* access to a standard chow diet (Maintenance 3432, KLIBA NAFAG, Kaiseraugst, Switzerland) and water. The temperature was maintained constantly between 21 and 22°C. Upon completion of experiments, animals were killed through gradual CO₂ overdose, and death was ensured by terminal bleeding. Tissues collected from the mice were snap-frozen in liquid nitrogen for downstream analyses.

Body composition analysis

Body composition was assessed with an EchoMRI-100 analyser (EchoMRI Medical Systems). Fat and lean mass were normalized to total body mass.

Body temperature and locomotor activity recordings

General locomotor activity and core body temperature data were acquired with the E-Mitter Telemetry System (Starr Life Sciences) from single-caged animals placed in an environment-controlled cabinet (UniProtect Air

Flow Cabinet, Bioscape). Briefly, small transponders (G2 E-Mitter, Starr Life Sciences) were implanted into the abdominal cavity of mice under isoflurane anaesthesia (2% isoflurane + O₂). Mice were treated with meloxicam (1 mg/kg) pre- and postoperatively and allowed to recover for 3 weeks. The above-mentioned parameters, together with the wheel-running activity, were recorded with a PC-based acquisition system connected to ER4000 Receivers (VitalView, Starr Life Sciences).

Comprehensive laboratory animal monitoring system

A comprehensive animal metabolic monitoring system (CLAMS; Columbus Instruments) was used to evaluate food consumption, oxygen consumption (\dot{V}_{O_2}), and CO₂ production from singly housed mice within an environment-controlled cabinet with the temperature set at 23°C. Feeding was measured by recording the difference in the scale measurement of the centre feeder from one time point to another. We studied eight mice per genotype, after acclimation of 2 days.

Treadmill

Sedentary mice were acclimatized to the treadmill (Columbus Instruments, Columbus, OH, USA) on 3 consecutive days prior to starting the experiment. The acclimatization period consisted of the following intervention: day 1, placing the mice in the treadmill for 10 min without speed, followed by 5 min at 5 m/min; day 2, running at 5, 7 and 10 m/min for 5 min each; and day 3, running at 8, 10 and 12 m/min for 5 min each. All acclimatization runs were performed between zeitgeber time 2 (ZT2) and zeitgeber time 6 (ZT6). After resting for 1 day, a maximal exercise capacity test was performed by 3 min at 8 m/min, increasing treadmill speed by 2 m every 2 min until the speed of 32 m/min, then increasing treadmill speed by 2 m every 5 min until exhaustion was reached. The treadmill was maintained at a 15° slope throughout the test. The criterion for exhaustion was met if an animal remained on the electrical grid (providing a mild electrical stimulus of 0.5 mA, 200 ms pulse, 1 Hz) for more than 5 s. Tail blood glucose (Accu-Chek, Roche) and lactate (Lactate Plus meter, Nova Biomedical) values were determined immediately before treadmill exercise and within 1 min after physical exhaustion. These tests were performed between ZT2 and ZT6 for the daytime measurements and between ZT16 and ZT20 for the night-time measurements.

Muscle tissue preparation and blood collection

Mice from the different experiments were killed by short exposure to CO₂ and immediate exsanguination. Blood

was collected in tubes containing lithium heparin (Microvette 500 LH, Sarstedt, 20.1345) centrifuged at 2000g for 5 min at room temperature and stored at -80°C . Various skeletal muscle tissues (quadriceps, tibialis anterior, soleus, gastrocnemius, plantaris and diaphragm) and tissues such as heart, liver, kidney and adipose tissue were collected and quickly snap-frozen in liquid nitrogen. The samples were stored at -80°C until further analysis. Validation of the knockdown of PER2 and ROR α in the respective animal models was tested in all the tissues collected. In addition, for all RNA-related assays, such as qPCRs and RNA sequencing (RNA-seq), the gastrocnemius muscles were used. For histology, the quadriceps, tibialis anterior and soleus muscles were used. Data from the tibialis anterior muscle are shown in the manuscript.

Quantitative real-time PCR

Total RNA from the gastrocnemius muscle tissues was extracted using a hybrid method combining TRI-Reagent (Sigma-Aldrich T9424) and the RNeasy Mini Kit (QIAGEN 74104). The quantity and purity of the RNA were measured with a NanoDrop OneC (ThermoFisher Scientific). The High-Capacity cDNA Reverse Transcript Kit (Applied Biosystems, 4368814) was used for cDNA synthesis with 1 μg of total RNA. Quantitative real-time PCR was performed with Fast SYBR Green Master Mix (Applied Biosystems, 4385612) in an RT-PCR System (StepOnePlus, Applied Biosystems). PCRs were done in duplicate with the addition of negative controls (i.e. no reverse transcription and no template controls). Relative expression levels were determined using the comparative ΔCT method to normalize target gene mRNA to *Hprt*. Primers were designed and tested as previously described (Delezie et al., 2012).

Tryptic digest, TMT labelling and liquid chromatography–tandem mass spectrometry analysis

Muscle tissue was pulverized and lysed in 1% sodium deoxycholate, 10 mM Tris(-2carboxyethyl)phosphine (TCEP), 100 mM Tris (pH 8.5) by sonication (Bioruptor, 20 cycles, 30 s on–30 s off, Diagenode, Belgium). Samples were incubated for 10 min at 95°C , allowed to cool down to room temperature, followed by the addition of chloroacetamide at a final concentration of 15 mM. After an incubation of 30 min at 37°C , sequencing-grade modified trypsin (1/50, w/w; Promega, Madison, WI, USA) was added, and proteins were digested for 12 h at 37°C , shaking at 300 r.p.m. Digests were acidified (pH < 3) using trifluoroacetic acid (TFA) and desalted using iST cartridges (PreOmics, Martinsried, Germany) according to the manufacturer's instructions. Peptides were dried under vacuum and stored at -20°C .

Sample aliquots comprising 25 μg of peptides were labelled with isobaric tandem mass tags (TMT 10-plex, Thermo Fisher Scientific) as described previously (Ahrné et al., 2016). Briefly, peptides were resuspended in 20 μl of labelling buffer (2 M urea and 0.2 M Hepes, pH 8.3), and 5 μl of each TMT reagent was added to the individual peptide samples, followed by a 1 h incubation at 25°C . To control for ratio distortion during quantification, a peptide calibration mixture consisting of six digested standard proteins mixed in different amounts was added to each sample before TMT labelling. To quench the labelling reaction, 1.5 μl of aqueous 1.5 M hydroxylamine solution was added, and samples were incubated for another 10 min at 25°C , followed by pooling of all samples. The pH of the sample pool was increased to 11.9 by adding 1 M phosphate buffer (pH 12) and incubated for 20 min at 25°C to remove TMT labels linked to peptide hydroxyl groups. Subsequently, the reaction was stopped by adding 2 M hydrochloric acid until a pH < 2 was reached. Finally, peptide samples were acidified further using 5% TFA, desalted using Sep-Pak Vac 1cc (50 mg) C18 cartridges (Waters) according to the manufacturer's instructions, dried under vacuum and stored at -20°C .

The TMT-labelled peptides were fractionated by high-pH reversed phase separation using a XBridge Peptide BEH C18 column (3.5 μm , 130 \AA , 1 mm \times 150 mm, Waters) on an Agilent 1260 Infinity HPLC system. Peptides were loaded on the column in buffer A (20 mM ammonium formate in water, pH 10) and eluted using a two-step linear gradient from 2% to 10% in 5 min and then to 50% buffer B (20 mM ammonium formate in 90% acetonitrile, pH 10) over 55 min at a flow rate of 42 $\mu\text{l}/\text{min}$. Elution of peptides was monitored with an ultraviolet detector (at 215 and 254 nm), and a total of 36 fractions were collected, pooled into 12 fractions using a post-concatenation strategy as previously described (Wang et al., 2011) and dried under vacuum.

Dried peptides were resuspended in 0.1% aqueous formic acid and subjected to liquid chromatography–tandem mass spectrometry analysis using a Q Exactive HF Mass Spectrometer fitted with an EASY-nLC 1000 (both from Thermo Fisher Scientific) and a custom-made column heater set to 60°C . Peptides were resolved using an RP-HPLC column (75 μm \times 30 cm) packed in-house with C18 resin (ReproSil-Pur C18-AQ, 1.9 μm resin; Dr Maisch GmbH) at a flow rate of 0.2 $\mu\text{l}/\text{min}$. The following gradient was used for peptide separation: from 5% B to 15% B over 10 min to 30% B over 60 min to 45% B over 20 min to 95% B over 2 min, followed by 18 min at 95% B. Buffer A was 0.1% formic acid in water, and buffer B was 80% acetonitrile, 0.1% formic acid in water.

The mass spectrometer was operated in DDA mode, with a total cycle time of ~ 1 s. Each MS1 scan was followed by high-collision–dissociation (HCD) of the 10 most

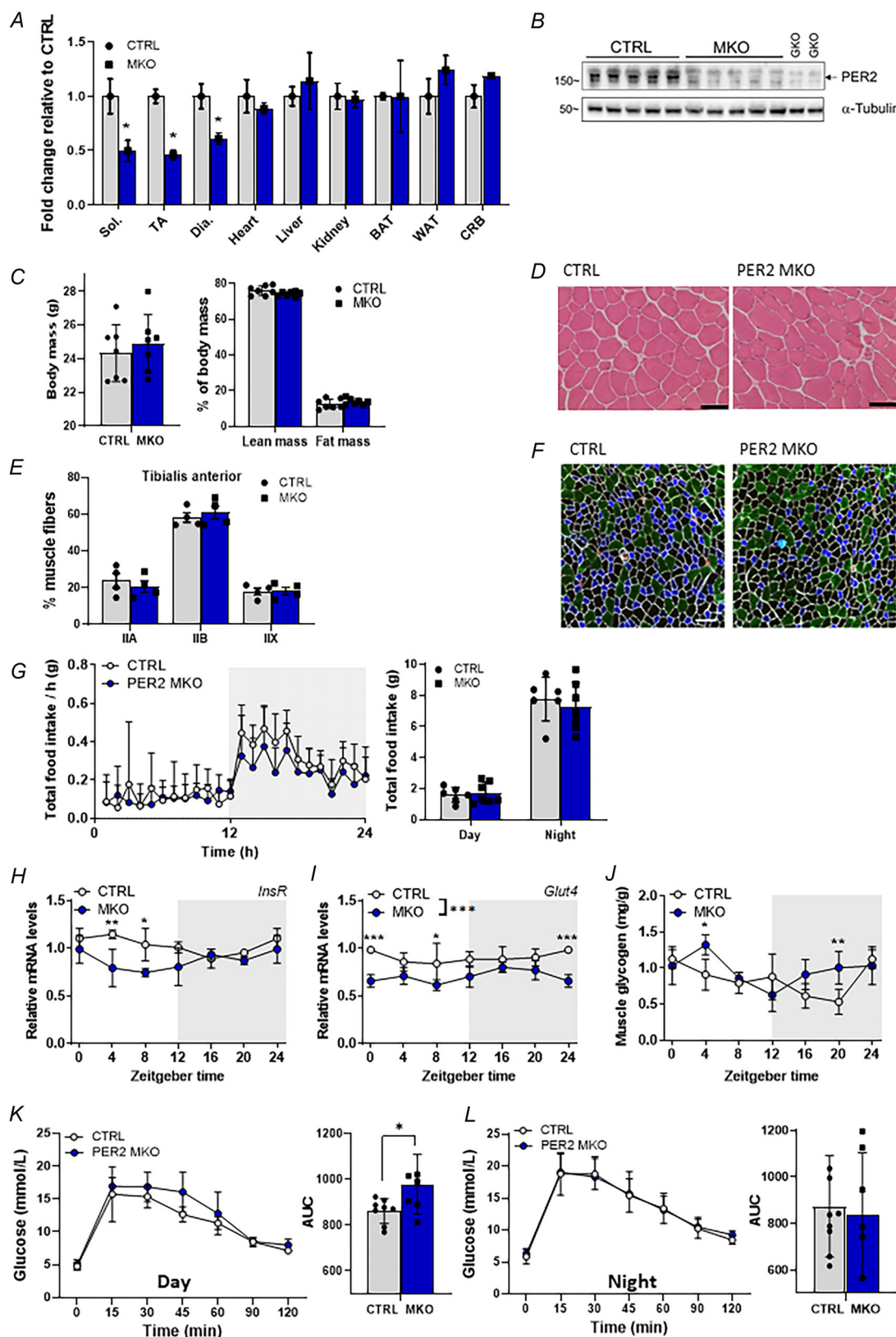


Figure 1. Validation of PER2 deletion in skeletal muscle and characterization of physiological parameters. *A*, quantitative PCR (qPCR) analysis showing the fold change of *Per2* mRNA in PER2 muscle-specific knockout (MKO) mice relative to control littermates (CTRL). *B*, western blot confirming the deletion of PER2 protein in

the gastrocnemius muscle of PER2 MKO mice. *C*, comparison of absolute body mass, lean mass and fat mass percentages between PER2 MKO and CTRL. *D*, Haematoxylin and Eosin staining of skeletal muscle sections from PER2 MKO and control mice. Scale bars: 50 μ m. *E*, quantification of fibre types in MKO and control mice from immunofluorescence image analysis of muscle sections. *F*, representative immunofluorescence images of muscle sections. Scale bar: 100 μ m. *G*, comparison of total food intake per hour over a period of 24 h in *ad libitum* feeding conditions. The bar graph shows the total food intake from 0 to 12 h (day) and 12 to 24 h (night). *H*, mRNA levels of insulin receptor (*InsR*) measured by qPCR in the gastrocnemius muscle over 4 h intervals. *I*, mRNA levels of glucose transporter (*Glut4*) measured by qPCR in the gastrocnemius muscle over 4 h intervals. *J*, muscle glycogen concentration (in milligrams per gram) in the gastrocnemius muscle over 4 h intervals. *K* and *L*, blood glucose levels (in millimoles per litre) measured every 15 min after i.p. glucose injection, at ZT4 (day; *K*) and ZT16 (night; *L*). The bar graphs show the area under the curve over the 3 h (120 min) period. Light and dark periods are depicted by white and grey background, respectively. Abbreviations: BAT, adipose tissue; CB, cerebellum; Dia, diaphragm; Gas, gastrocnemius; Plan, plantaris; Sol, soleus; TA, tibialis anterior; WAT, white adipose tissue. $n = 4$ per genotype for *A* and *B*; $n = 7$ or 8 per genotype for *C*–*G*. Results are expressed as the mean \pm SD; bar graphs show individual data points. * $q < 0.05$, ** $q < 0.01$ and *** $q < 0.001$; Student's unpaired *t* test or two-way ANOVA with Sidak's multiple comparisons test. [Colour figure can be viewed at wileyonlinelibrary.com]

abundant precursor ions, with dynamic exclusion set to 30 s. For MS1, 3×10^6 ions were accumulated in the Orbitrap over a maximum time of 100 ms and scanned at a resolution of 120,000 full width at half maximum (at 200 *m/z*). MS2 scans were acquired at a target setting of 1×10^5 ions, maximum accumulation time of 100 ms and a resolution of 30,000 full width at half maximum (at 200 *m/z*). Singly charged ions and ions with unassigned charge state were excluded from triggering MS2 events. The normalized collision energy was set to 35%, the mass isolation window was set to 1.1 *m/z*, and one microscan was acquired for each spectrum.

The acquired raw files were converted to the mascot generic file (mgf) format using the msconvert tool [part of ProteoWizard, v.3.0.4624 (2013-6-3)] and searched using MASCOT against a murine database (consisting of 49,434 forward and reverse protein sequences downloaded from Uniprot), the six calibration mix proteins (Ahrné et al., 2016) and 390 commonly observed contaminants. The precursor ion tolerance was set to 10 p.p.m., and fragment ion tolerance was set to 0.02 Da. The search criteria were set as follows: full tryptic specificity was required (cleavage after lysine or arginine residues unless followed by proline); three missed cleavages were allowed; and carbamidomethylation (C) and TMT6plex (K and peptide N-terminus) were set as fixed modification and oxidation (M) as a variable modification. Next, the database search results were imported into the Scaffold Q+ software (v.4.3.2, Proteome Software, Portland, OR, USA), and the protein false-discovery rate was set to 1%. Proteins that contained similar peptides and could not be differentiated based on tandem mass spectrometry analysis alone were grouped to satisfy the principles of parsimony. Proteins sharing significant peptide evidence were grouped into clusters. Acquired reporter ion intensities in the experiments were used for automated quantification and statistical analysis with a modified version of our in-house-developed SafeQuant R script (v.2.3; Ahrné et al., 2016). This analysis included adjustment of reporter ion intensities, global

data normalization by equalizing the total reporter ion intensity across all channels, summation of reporter ion intensities per protein and channel, calculation of protein abundance ratios, and testing for differential abundance using empirical Bayes-moderated *t*-statistics.

RNA sequencing and data analysis

Total RNA from the gastrocnemius muscle tissues was extracted using a hybrid method combining TRI-Reagent (Sigma-Aldrich T9424) and the RNeasy Mini Kit (QIAGEN 74104). The quality of RNA was determined on the Bioanalyzer instrument (Agilent Technologies, Santa Clara, CA, USA) using the RNA 6000 Nano Chip [Agilent, catalogue number (Cat#) 5067-1511] and quantified by spectrophotometry using the NanoDrop ND-1000 Instrument (NanoDrop Technologies, Wilmington, DE, USA). Library preparation was performed with 1 μ g total RNA using the TruSeq Stranded mRNA Library Prep Kit High Throughput (Cat# RS-122-2103, Illumina, San Diego, CA, USA). Libraries were quality checked on the Fragment Analyzer (Advanced Analytical, Ames, IA, USA) using the Standard Sensitivity NGS Fragment Analysis Kit (Cat# DNF-473, Advanced Analytical), revealing excellent quality of libraries (average concentration was 152 ± 9 nmol/l, and average library size was 374 ± 4 bp). Samples were pooled to equal molarity. Each pool was quantified by PicoGreen Fluorometric measurement in order to be adjusted to 1.8 μ M and used for clustering on the NextSeq 500 instrument (Illumina). Samples were sequenced single-end, 76 base read length using the NextSeq 500 High Output Kit 75-cycles (Illumina, Cat# FC-404-1005), and primary data analysis was performed with the Illumina RTA v.2.4.11 and Basecalling v.bcl2fastq-2.20.0.422.

Secondary data analysis included performing an initial quality control assessment (Ewels et al., 2016), after which sequenced reads were mapped onto GRCm39 mouse genomes ENSEMBL v.104 using the software STAR

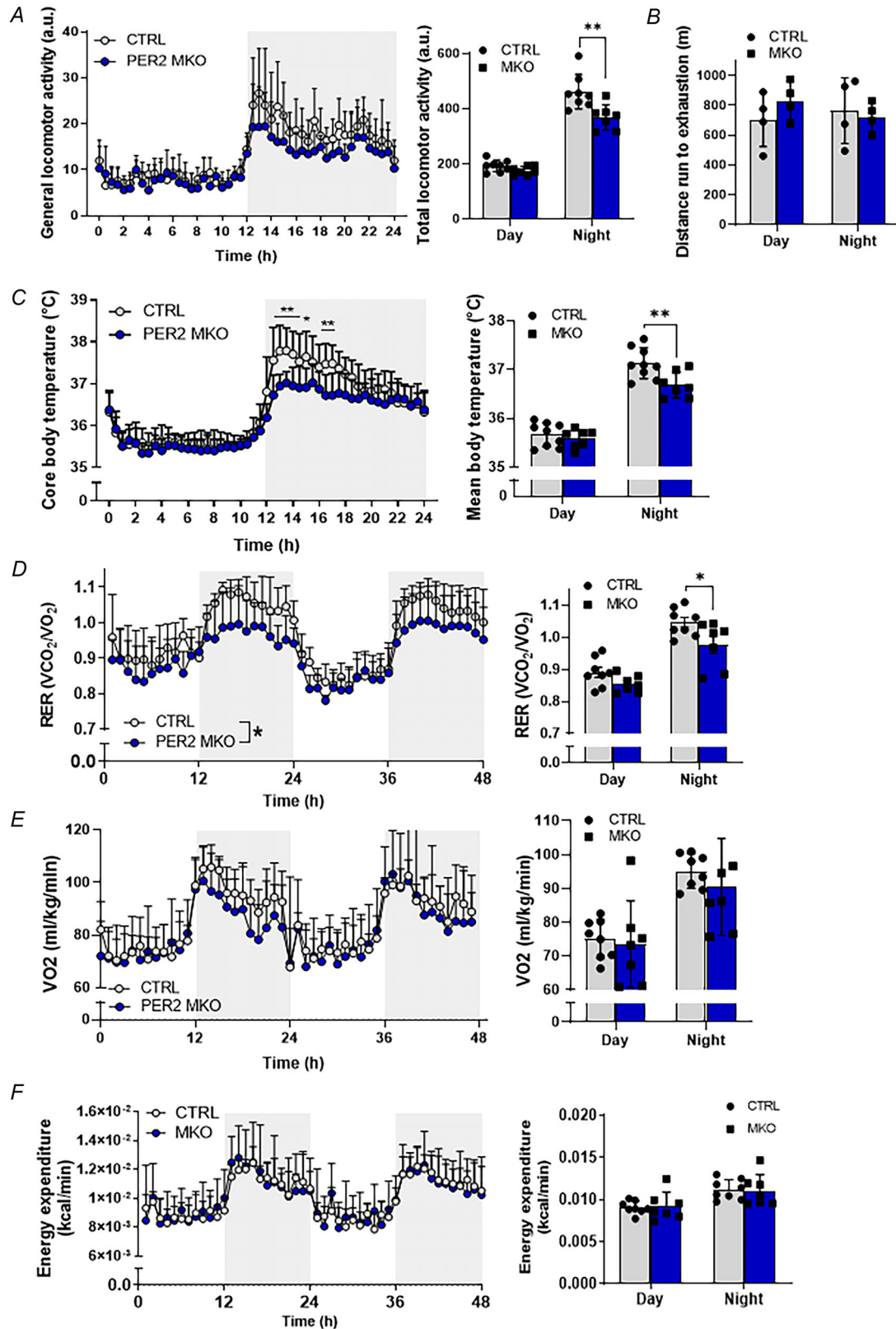


Figure 2. Characterization of functional and metabolic parameters in PER2 muscle-specific knockout mice

A, voluntary locomotor activity of control and PER2 muscle-specific knockout (MKO) mice measured over 4 days and averaged over a 24 h period in arbitrary units (a.u.). The bar graph shows the average from 0 to 12 h (day)

and 12–24 h (night). *B*, maximal treadmill running capacity of control and PER2 MKO mice assessed at zeitgeber time 4 (ZT4, daytime) and zeitgeber time 20 (ZT20, night-time). *C*, core body temperature measured over 4 days and averaged over a 24 h period. The bar graph shows the average from 0 to 12 h (day) and 12 to 24 h (night). *D*, respiratory exchange ratio (RER) measured over 48 h. The bar graph shows the average over 12 h periods. *E*, rate of volume of oxygen consumption (\dot{V}_{O_2}) measured over 48 h. The bar graph shows the averaged values over 12 h periods. *F*, energy expenditure (in kilocalories per minute) measured over 48 h. The bar graph shows the average over 12 h periods. Light and dark periods are depicted by white and grey background, respectively. $n = 7$ or 8 per genotype for A–E. Results are expressed as the mean \pm SD; bar graphs show individual data points. * $q < 0.05$, ** $q < 0.01$; Student's unpaired *t* test or two-way ANOVA with Sidak's multiple comparisons test. [Colour figure can be viewed at wileyonlinelibrary.com]

(Dobin et al., 2013). Both raw and trimmed reads [trimmomatic (Bolger et al., 2014), with the option LEADING:15 TRAILING:15 SLIDINGWINDOW:4:15] were aligned; the raw reads yielded more uniquely mapped reads and were thus kept for the rest of the analysis. Gene expression levels were assessed using STAR with the '-quantMode GeneCounts' option. Differential analysis was performed using the software R (v.4.1) with the DESeq2 library (Love et al., 2014). Only genes with ≥ 10 reads in at least three samples (equivalent to the number of replicates) were kept. Each biological replicate was used to produce two technical replicates, which were sequenced in separate lanes; this information was integrated to the DESeq2 model in order to account for a potential batch effect. A false-discovery rate threshold of 0.01 was used to declare genes as differentially expressed (DE). Similarity between sets of DE genes was visualized with the upsetR package (Conway et al., 2017).

For circadian analysis of the data, the standard software tximport was used to go from transcript-level abundances to gene-level ('flat') abundances. Abundances were measured in estimated counts using countsFromAbundance = 'lengthScaledTPM' in the tximport function. Counts were then normalized using the variance stabilizing transformation (VST) procedure of the DESeq2 package, to achieve roughly equal variances for each time point. When comparing genes against each other (intergenic comparisons), we instead used abundances measured in tags per million (TPM), which corrects for differences in gene lengths (without such correction, long genes will tend to exhibit higher counts than shorter genes at the same expression level), but which does not allow VST normalization. The TPM values were used for the cut-offs determining which genes are expressed and which are not. Resulting transcript abundance estimates using the TPM measure (suitable for comparing different transcripts/genes with each other) showed a standard distribution.

The *P*-value distributions for algorithms such as JTK Cycle or rhythmicity analysis incorporating non-parametric methods (RAIN), which detect circadian rhythmicity, are bimodal; hence, we adjusted the RAIN *P*-values with the standard Benjamini–Hochberg method. The quantifications were tested for circadian rhythms using the published method, RAIN. We focused on genes

with amplitudes of >0.1 either in control (CTRL) or KO animals, and combined *P*-values of CTRL and KO using *P*-value meta-analysis, in order to define circadian genes. Furthermore, DE analysis was carried out using a robust regression model taking circadian rhythms into account, such that DE refers to the robust means of the possibly rhythmic expression patterns. Finally, differential rhythmicity (DR) was tested for the circadian genes, using the detection of differential rhythmicity (DODR) R package, available on CRAN (Thaben & Westermarck, 2016). This test is complementary to the DE test; here, only differences in rhythmicity (relative/fold change amplitude and/or phase difference) were tested, allowing for and compensating for differences in mean expression levels.

Pathway enrichment analysis

Reactome pathway enrichment analysis was performed using DAVID (Huang et al., 2009; Sherman et al., 2022) for the proteomic and transcriptomic datasets. Transcription factor enrichment analysis was performed using the Web-based tool ChEA3 (Keenan et al., 2019). Note that our input lists contained all transcripts or proteins of a given mouse group at a given time point meeting statistical thresholds of $P \leq 0.05$ for proteomic data and false-discovery rate ≤ 0.05 for transcriptomic data.

Metabolomics

Metabolites were extracted from 50 mg of muscle tissue from five or six mice per time point (ZT4 and ZT16) and per genotype (PER2 or ROR α MKO) using the MxP[®] Quant 500 kit. The samples were then sent to Biocrates Life Sciences AG for metabolic profiling. Data on >630 metabolites were received in the form of EExcel files from the company, which were then used for downstream analyses.

Statistical analysis

The number (*n*) used per genotype for each experiment is indicated in the figure legends. Data are represented as the mean \pm SD and analysed statistically with GraphPad

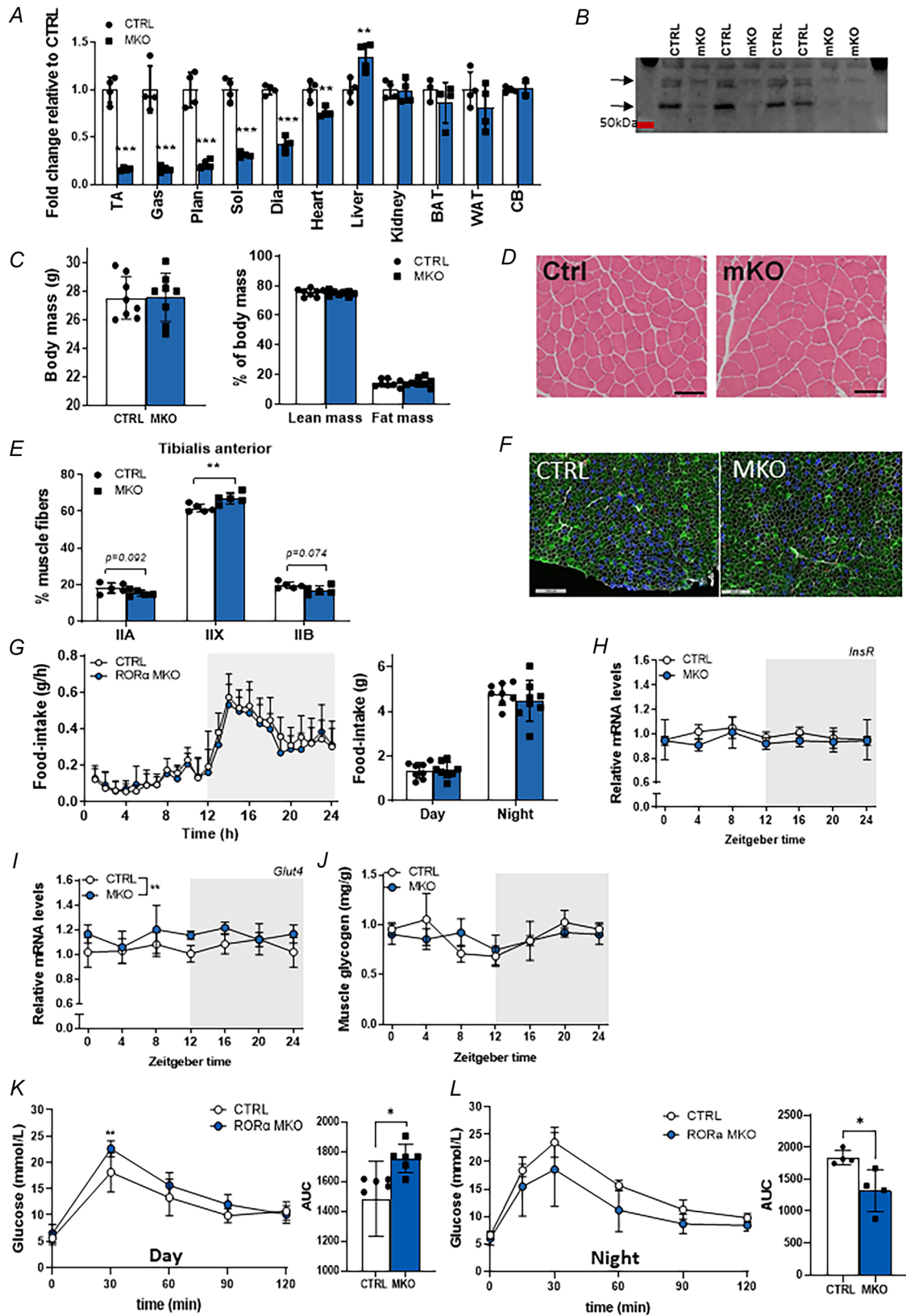


Figure 3. Validation of ROR α deletion in skeletal muscle and characterization of physiological parameters

A, quantitative PCR (qPCR) analysis showing the fold change of *Ror α* mRNA in ROR α muscle-specific knockout (MKO) mice relative to control littermates (CTRL). *B*, western blot confirming the deletion of ROR α protein in the

gastrocnemius muscle. *C*, comparison of absolute body mass, lean mass and fat mass percentages between ROR α MKO and CTRL. *D*, Haematoxylin and Eosin staining of skeletal muscle sections from MKO and control mice. Scale bars: 50 μ m. *E*, quantification of fibre types in ROR α MKO and control mice from immunofluorescence image analysis of muscle sections. *F*, representative immunofluorescence images of muscle sections. Scale bars: 300 μ m. *G*, comparison of total food intake per hour over a period of 24 h in *ad libitum* feeding conditions. The bar graph shows the total food intake from 0 to 12 h (day) and 12 to 24 h (night). *H*, mRNA levels of insulin receptor (*InsR*) measured by qPCR in the gastrocnemius muscle over 4 h intervals. *I*, mRNA levels of glucose transporter (*Glut4*) measured by qPCR in the gastrocnemius muscle over 4 h intervals. *J*, muscle glycogen concentration (in milligrams per gram) in the gastrocnemius muscle over 4 h intervals. *K* and *L*, blood glucose levels (in millimoles per litre) measured every 15 min after i.p. glucose injection, at zeitgeber time 4 (ZT4; daytime, *K*) and zeitgeber time 16 (ZT16; night-time, *L*). The bar graphs show the area under the curve over a 3 h (120 min) period. Light and dark periods are depicted by white and grey background, respectively. Abbreviations: BAT, adipose tissue; CB, cerebellum; Dia, diaphragm; Gas, gastrocnemius; Plan, plantaris; Sol, soleus; TA, tibialis anterior; WAT, white adipose tissue. $n = 4$ per genotype for *A* and *B*; $n = 7$ or 8 per genotype for *C*–*G*. Results are expressed as the mean \pm SD; bar graphs show individual data points. * $q < 0.05$, ** $q < 0.01$ and *** $q < 0.001$; Student's unpaired *t* test or two-way ANOVA with Sidak's multiple comparisons test. [Colour figure can be viewed at wileyonlinelibrary.com]

Prism 8. Student's *t* test was performed to evaluate statistical differences between the two groups. For multiple comparisons, data were analysed using two-way ANOVA followed by Sidak's multiple comparisons test. Corresponding symbols to highlight statistical significance are as follows: * $q \leq 0.05$, ** $q \leq 0.01$ and *** $q \leq 0.001$.

Results

Muscle-specific PER2 deletion leads to time of day-dependent alterations in activity and metabolic capacity

Deletion of PER2 in skeletal muscle was achieved by crossing mice harbouring a floxed *Per2* allele with mice that express Cre recombinase under the control of the skeletal muscle-specific HSA-promoter, as described in the Methods. These mice are hereafter referred to as PER2 MKO. The efficiency of the deletion of PER2 was verified in various skeletal muscles, and the specificity validated in non-muscle tissues by qPCR of *Per2* mRNA (Fig. 1A). Furthermore, the KO was confirmed at the protein level by western blotting gastrocnemius muscle extracts (Fig. 1B). There were no differences in absolute body mass or in lean and fat mass percentages between the PER2 MKO and control mice (Fig. 1C). The general morphology of the muscle was unaffected, as determined by Haematoxylin and Eosin staining (Fig. 1D), and the fibre-type composition was also unchanged between the two groups (Fig. 1E and F). In *ad libitum* conditions, daily food intake was similar in wild-type (WT) controls and PER2 MKOs (Fig. 1G). Muscle mRNA levels of insulin receptor (*InsR*) were significantly downregulated in the PER2 MKOs during the inactive phase (Fig. 1H), and mRNA levels of the insulin-regulated glucose transporter, *Glut4*, were significantly downregulated in both active and inactive phases (Fig. 1I). Total muscle glycogen levels were higher at peak inactive (ZT4) and active phase

(ZT20) in the PER2 MKOs (Fig. 1J). Consequently, PER2 MKO mice exhibited lower glucose tolerance during the day compared with control littermates (Fig. 1K), with no differences in night-time glucose tolerance (Fig. 1L). This is in line with previous studies that observed reduced fasting glycaemia and impaired gluconeogenesis in *Per2*-mutant mice (Schmutz et al., 2010; Zani et al., 2013; Zhao et al., 2012). It is interesting to note that these impairments in glucose metabolism were largely attributed to the liver-intrinsic clock, whereas we show that such changes can also be driven by the muscle-intrinsic modulation of *Per2*.

We then sought to investigate whether there were differences in activity or substrate utilization in the PER2 MKOs. General locomotor activity did not differ between the control littermates and PER2 MKO mice during the day (light period; resting/inactive phase), but was significantly reduced in the MKO mice during the night (dark period; feeding/active phase) (Fig. 2A). To assess whether PER2 deletion affected exercise performance, we challenged the two groups of mice with a maximal performance test. Interestingly, there were no significant changes in the maximal treadmill running capacity of the PER2 MKO mice compared with their control littermates at either ZT4 (daytime) or ZT20 (night-time) (Fig. 2B), indicating that deletion of PER2 in the muscle reduces night time-specific voluntary activity without affecting exercise capacity. In accordance with reduced activity, the core body temperature of the MKO mice was also significantly lower at night-time and unchanged in the daytime (Fig. 2C). The decrease in the respiratory exchange ratio (RER) of the MKO mice (Fig. 2D) was not driven by a modulation of \dot{V}_{O_2} (Fig. 2E), nevertheless indicating that the MKO mice might depend more on lipid oxidation than their control littermates. Alternatively, it might be that the MKO mice are less capable of switching from lipid oxidation in the fasted state to glucose oxidation in the fed state, indicating reduced metabolic flexibility in the muscle in the absence of PER2.

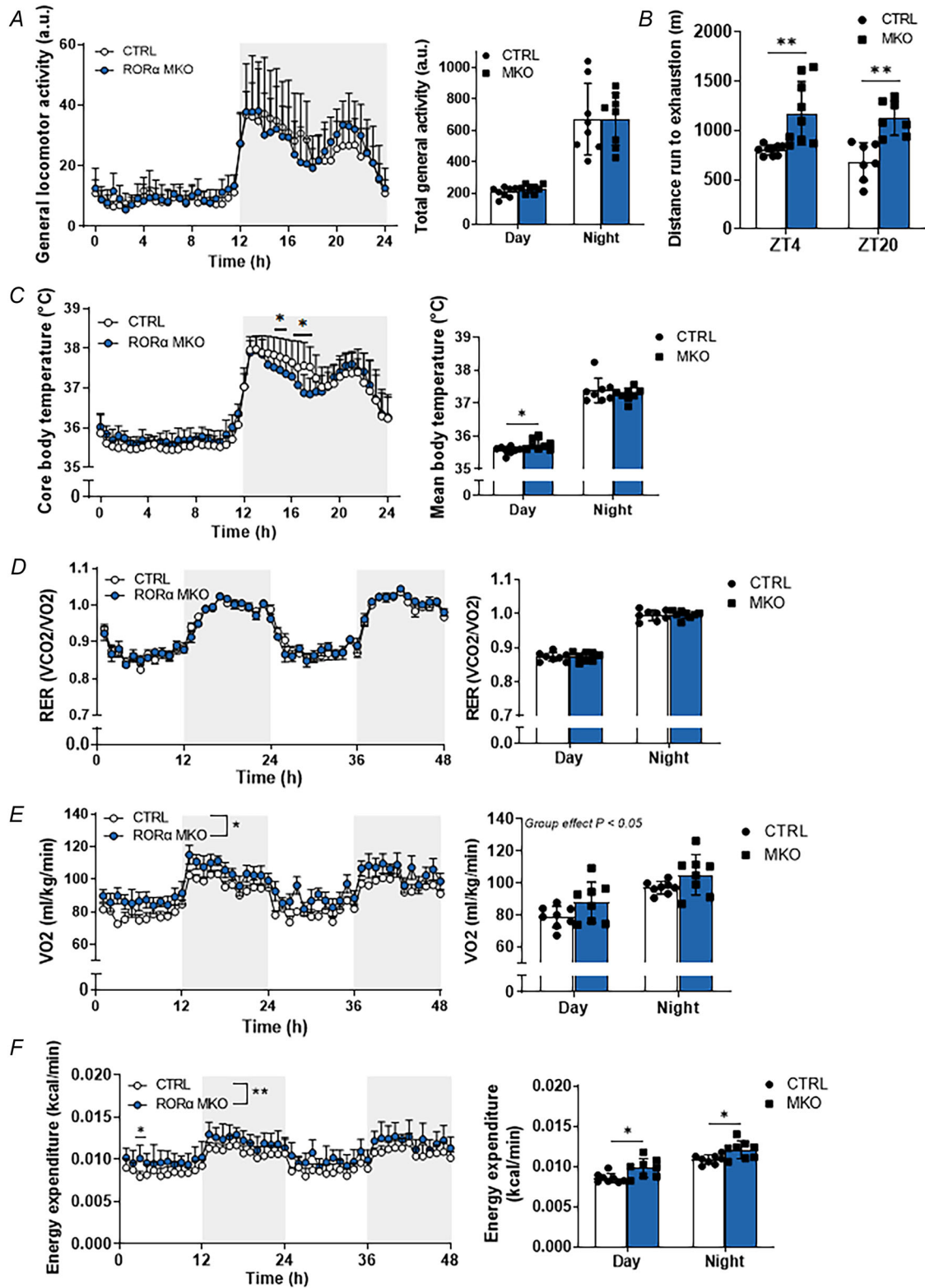


Figure 4. Characterization of functional and metabolic parameters in ROR α muscle-specific knockout mice

A, voluntary locomotor activity of control and ROR α muscle-specific knockout (MKO) mice measured over 4 days and averaged over 24 h. The bar graph shows the average from 0 to 12 h (day) and 12 to 24 h (night). **B**, maximal treadmill running capacity of control and ROR α MKO mice assessed at zeitgeber time 4 (ZT4, daytime)

and zeitgeber time 20 (ZT20, night-time). C, core body temperature measured over 4 days and averaged over 24 h. The bar graph shows the average from 0 to 12 h (day) and 12 to 24 h (night). D, respiratory exchange ratio (RER) measured over 48 h. The bar graph shows the average over 12 h periods. E, oxygen consumption (\dot{V}_{O_2}) measured over 48 h. The bar graph shows the average over 12 h periods. F, energy expenditure (in kilocalories per minute) measured over 48 h. The bar graph shows the average over 12 h periods. Light and dark periods are depicted by white and grey backgrounds, respectively. $n = 7$ or 8 per genotype for A–E. Results are expressed as the mean \pm SD; bar graphs show individual data points. * $q < 0.05$, ** $q < 0.01$; Student's unpaired t test or two-way ANOVA with Sidak's multiple comparisons test. [Colour figure can be viewed at wileyonlinelibrary.com]

Muscle-specific ROR α deletion leads to alterations in exercise performance, metabolic capacity, energy balance and muscle fibre type

Deletion of ROR α in skeletal muscle was achieved by crossing mice encoding a floxed ROR α allele with mice that express Cre recombinase under the control of the skeletal muscle-specific HSA-promoter as described in the Methods. These mice are referred to hereafter as ROR α MKO. The deletion of ROR α was detected in all the skeletal muscles tested, in addition to a slight reduction in the heart and elevation in the liver, as determined by qPCR analysis of the *Ror α* mRNA (Fig. 3A). Deletion of the protein in the gastrocnemius muscle was validated by western blot (Fig. 3B). Absolute body mass and lean and fat mass percentages were unchanged between the MKO and control mice (Fig. 3C). The general morphology of the muscle was inconspicuous (Fig. 3D); however, the fibre-type composition of the tibialis anterior muscle was shifted towards more type 2X (fast-intermediate) fibres in the ROR α MKO mice (Fig. 3E and F). In *ad libitum* conditions, daily food intake was similar between the groups (Fig. 3G). Messenger RNA levels of insulin receptor (*InsR*) were unchanged (Fig. 3H), whereas mRNA levels of the insulin-regulated glucose transporter, *Glut4*, were significantly upregulated (Fig. 3I). However, the total muscle glycogen was unaffected (Fig. 3J). Intriguingly, ROR α MKO mice exhibited a phase shift in glucose tolerance, with lower glucose tolerance during the day compared with control littermates (Fig. 3K) and, inversely, higher glucose tolerance at night (Fig. 3L). Previous studies showed contrasting results, with improved insulin sensitivity and enhanced glucose uptake in skeletal muscle of *Ror α staggerer* (sg/sg) mice and mild hyperglycaemia and glucose intolerance with truncated ROR α expression in skeletal muscle (Lau et al., 2011; Raichur et al., 2010). Our data add temporal and tissue-specific insights to these results by showing ROR α -dependent modulation of glucose uptake in the skeletal muscle, which, coupled with substrate availability, leads to a phase shift in day and night glucose metabolism in the muscle.

General locomotor activity did not differ between the control littermates and the ROR α MKO mice (Fig. 4A), but when challenged in a maximal performance test on a treadmill, ROR α MKO mice showed significantly improved exercise capacity at both day (ZT4, rest phase) and night-time (ZT20, active phase) (Fig. 4B). The core body temperature of the ROR α MKO mice was increased

during the inactive phase and decreased between ZT17 and ZT18 (Fig. 4C). The RER of the ROR α MKO mice was comparable to their control littermates (Fig. 4D), despite significantly higher \dot{V}_{O_2} , independent of the time of day (Fig. 4E). In addition, ROR α MKO mice had higher energy expenditure independent of the time of day (Fig. 4F), which is in line with the increased \dot{V}_{O_2} observed.

PER2 and ROR α deletions lead to severe dampening of core clock gene oscillations

Given that PER2 and ROR α proteins are involved in the primary and secondary feedback loops of the circadian clock, respectively, we investigated the effect of PER2 and ROR α deletion on the expression and oscillation of core clock and closely associated genes in the muscle by performing qPCRs at 4 h intervals over a 24 h period (ZT0, ZT4, ZT8, ZT12, ZT16 and ZT20). As expected, PER2 MKO mice showed a marked reduction in *Per2* mRNA at all time points except ZT0 and ZT4, when baseline expression of *Per2* is already low (Fig. 5A). There was no compensatory modulation of other isoforms of the Period family, such as *Per1* and *Per3*. PER2 deletion also resulted in a slight downregulation of albumin D box-binding protein (*Dbp*), circadian locomotor output cycles kaput (*Clock*), cryptochrome 2 (*Cry2*), and *Ror α* mRNA at all time points and of retinoic acid receptor-related receptor γ (*Ror γ*) and nuclear receptor subfamily 1 group D member 1 (*Nr1d1*, *Rev-Erb α*) at ZT8 and ZT4, respectively (Fig. 5A). The expression of brain and muscle arnt-like 1 (*Bmal1*), cryptochrome 1 (*Cry1*) and nuclear receptor subfamily 1 group D member 2 (*Nr1d2*, *Rev-Erb β*) was unaffected (Fig. 5A).

The deletion of ROR α had large effects on circadian gene expression independent of the time of day (Fig. 5B). Apart from the expected downregulation of *Ror α* mRNA, we observed significantly decreased transcription of almost all clock genes at all time points, except for *Clock*, *Per1* and *Ror γ* , with the last being the only gene that showed increased expression levels (Fig. 5B).

Muscle-specific PER2 deletion elicits distinct, time-dependent transcriptomic changes in skeletal muscle

To gain a better understanding of which muscle-intrinsic gene networks could be impacted upon perturbation of

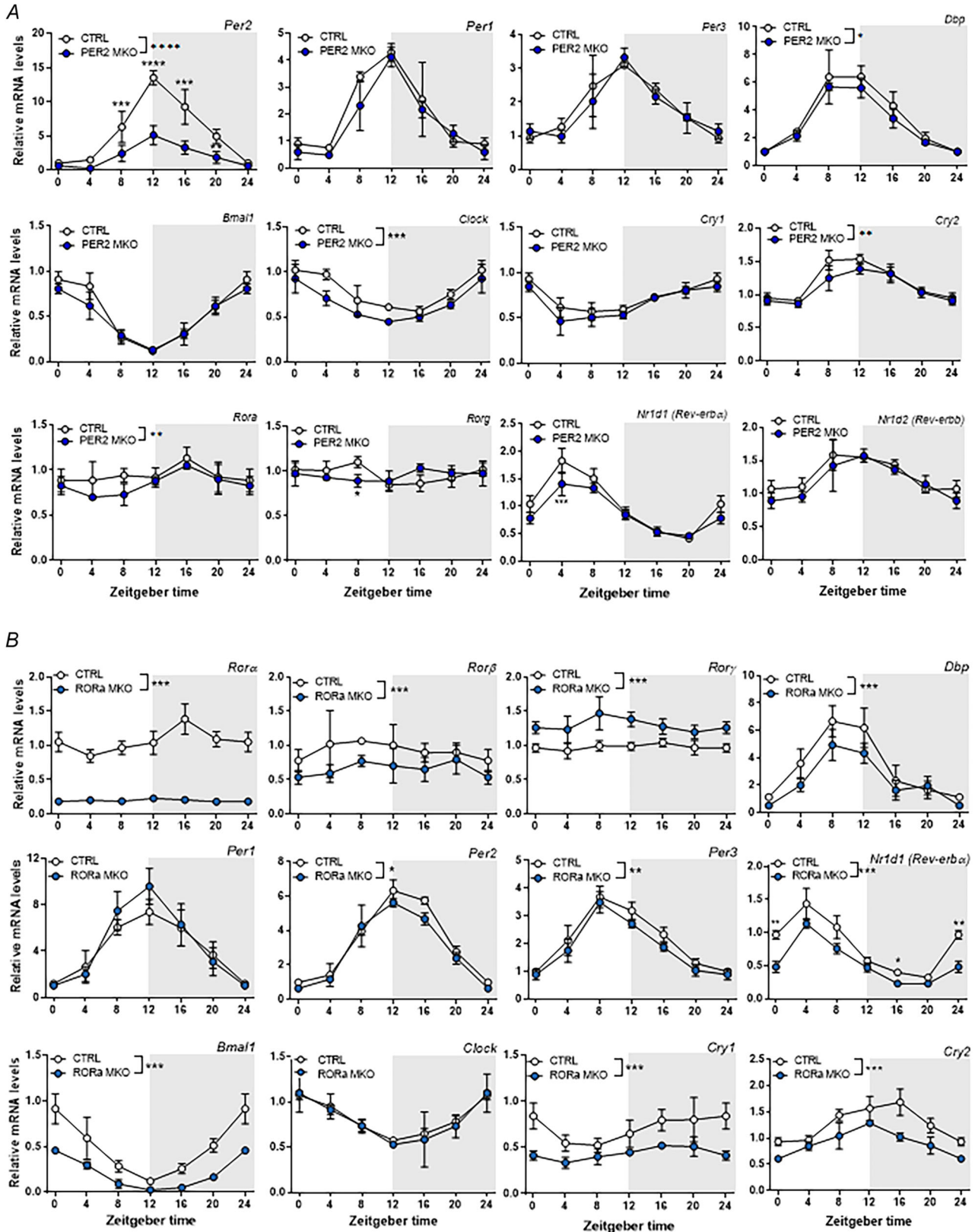


Figure 5. Effect of PER2 and ROR α deletion on core clock gene expression and oscillation in skeletal muscle
 A, core clock gene expression in PER2 muscle-specific knockout (MKO) mice: qPCR of core clock-regulating genes in skeletal muscle of PER2 MKO and control mice (CTRL). B, core clock gene expression in ROR α MKO mice: qPCR

of core clock-regulating genes in skeletal muscle of ROR α MKO and CTRL. Light and dark periods are depicted by white and grey backgrounds, respectively. Data are shown as the mean fold change \pm SD; bar graphs show individual data points ($n = 4$) relative to the expression in CTRL, zeitgeber time 0 (ZT0) set to one. * $q < 0.05$, ** $q < 0.01$, *** $q < 0.001$ and **** $q < 0.0001$; two-way ANOVA with Sidak's multiple comparisons test or Student's unpaired t test. [Colour figure can be viewed at wileyonlinelibrary.com]

the clock feedback loops, we looked at the transcriptional response to the deletion of PER2 in the muscle at distinct phases of the light–dark cycle. We performed RNA-seq gene expression profiling of muscles harvested at 4 h intervals over a 24 h period, namely at ZT0, ZT4, ZT8, ZT12, ZT16 and ZT20 (Fig. 6A–G).

Muscle-specific deletion of PER2 affected the muscle transcriptome in a very time of day-specific manner, with the greatest number of differentially expressed genes (DEGs) observed at ZT4 (Fig. 6C and H) and very few changes at all other time points (Fig. 6H). We applied non-parametric algorithms, such as RAIN and DODR, to this dataset to identify rhythmically oscillating genes between the different conditions (Fig. 6I). The output of the total number of rhythmically oscillating genes varies greatly depending on the cut-off used, and a detailed list of all these genes and their cut-off values can be found in Supplementary Table S1. Looking at all the circadian transcripts, we picked a RAIN cut-off of 0.10 and DODR cut-off of 0.25 to obtain 321 transcripts that were differentially regulated (DR) between the PER2 MKO and WT controls (Supplementary Table S1). Amplitude fold change estimations have large error margins, but seem to be centred on one (Fig. 6J), whereas the phase-change histogram hints at phase shifts to a few hours earlier in the KO animals (Fig. 6K). Interestingly, there was a large shift of transcripts with a morning phase in WT mice to a night/evening phase in the PER2 MKO and vice versa (Fig. 6L). Sixty-five genes were both differentially expressed and differentially regulated in a clock-dependent manner in the PER2 MKOs (Supplementary Table S1). An overlap between the transcriptome at all the different time points resulted in only 19 genes that were commonly upregulated in the PER2 MKOs at all ZTs (Fig. 6M) and 25 genes that were commonly downregulated at all ZTs (Fig. 6N), indicating that the transcriptomic response to PER2 deletion is largely specific to the time of day. The highest number of genes are upregulated at ZT4 (875), followed by ZT0 (178) and ZT12 (174), and the highest number of genes are downregulated at ZT4 (711), followed by ZT12 (258) and ZT0 (172) (Fig. 6M and N).

To dissect out the consequences of these changes on the circadian-associated metabolic/physiological functions, we focused on differences between the transcriptional responses at the two time points that induced the largest responses and fell within the inactive (ZT4) or active phase (ZT12) of the light–dark cycle. We performed reactome pathway enrichment and transcription factor

activity analysis to see which molecular pathways were differentially regulated at the two time points and what transcription factors were driving these changes (Fig. 7A–C). The only commonly upregulated pathway at both ZT4 and ZT12 was ‘detoxification of reactive oxygen species’ (Fig. 7A), with no overlap between the top 10 predicted transcription factors associated with the DEGs at each time point (Fig. 7B and C). At ZT4 specifically, there was a highly significant upregulation of terms related to metabolism, mitochondrial activity and translation (Fig. 7A). Pathways upregulated at other time points include ‘biological oxidations’ and ‘metabolism’ at ZT0, ‘signalling by Rho GTPases’ at ZT16, and ‘ascorbate and aldarate metabolism’ at ZT20 (Fig. 7D). Pathways that were transcriptionally downregulated in the PER2 MKOs showed a greater overlap, with terms such as ‘transport of amino acids/oligopeptides’ and ‘SLC-mediated transmembrane transport’ commonly downregulated not only at ZT4 and ZT12 (Fig. 7E) but also at ZT0, ZT8 and ZT20 (Fig. 7H). Of the top 10 predicted transcription factors driving the changes, PURA, ASH1L, MEF2A seem to be involved at both ZT4 and ZT12 (Fig. 7F and G).

Muscle-specific ROR α deletion profoundly affects skeletal muscle gene expression independent of the time of day

To gain a better understanding the transcriptional response to the deletion of ROR α in the muscle at distinct phases of the light–dark cycle, we performed RNA-seq of muscles harvested at 4 h intervals over a 24 h period, namely at ZT0, ZT4, ZT8, ZT12, ZT16 and ZT20 (Fig. 8A–G). ROR α deletion leads to massive differential regulation of the muscle transcriptome, with >1500 genes being differentially expressed at each of the time points analysed (Fig. 8H). We applied non-parametric algorithms, such as RAIN and DODR, to this dataset to identify rhythmically oscillating genes between the different conditions (Fig. 8I). The output of the total number of rhythmically oscillating genes varies greatly depending on the cut-off used, and a detailed list of all of these genes and their cut-off can be found in Supplementary Table 2. Looking at all the circadian transcripts, we picked a RAIN cut-off of 0.05 and DODR cut-off of 0.33 to obtain 283 transcripts that were differentially regulated (DR) between the ROR α MKO and WT controls (Supplementary Table S2). Similar to the PER2 MKOs, amplitude fold change estimations are centred on one

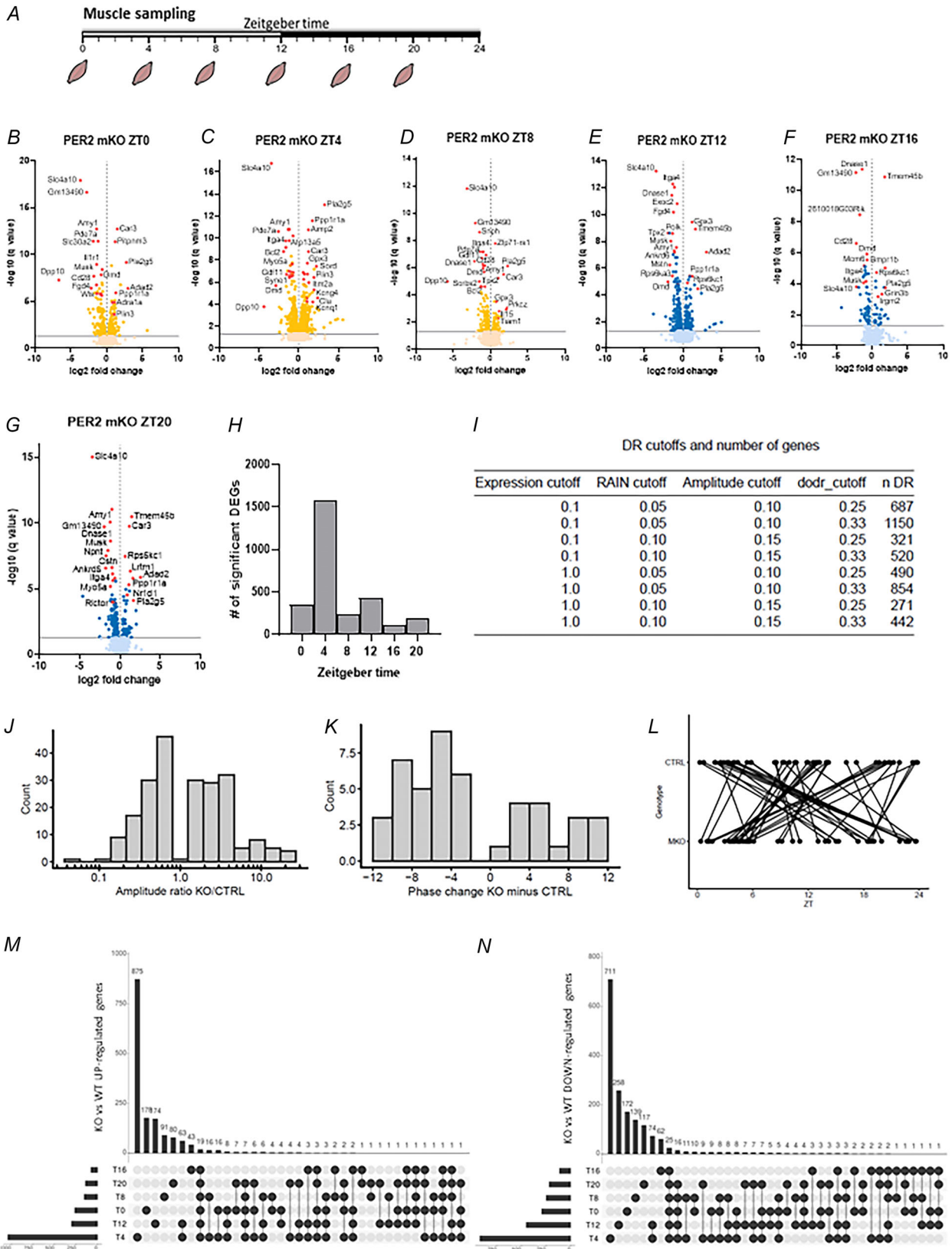


Figure 6. Time of day-specific transcriptional response to PER2 deletion in skeletal muscle
 A, schematic diagram of muscle sampling for RNA sequencing over 24 h. B–G, volcano plots displaying differentially expressed genes (DEGs) in PER2 muscle-specific knockout (MKO) mice relative to control mice (CTRL) at zeitgeber

time (ZT) 0, 4, 8, 12, 16 and 20. The top 15 genes are labelled in red. *H*, number of significant DEGs (cut-off, $P < 0.05$) at each time point. *I*, table with summary of differentially regulated (DR) transcripts obtained with different statistical cut-offs. *J*, histogram distribution of amplitude fold change estimations of the 321 DR circadian transcripts in KO vs. CTRL mice. *K*, histogram of phase changes of DR genes in KO vs. CTRL mice. *L*, transcript phase shift analysis showing the shift of gene transcript expression at different times. *M* and *N*, upset plots showing overlaps between upregulated (*M*) and downregulated (*N*) DEGs at different time points. Abbreviations: DODR, detection of differential rhythmicity; RAIN, rhythmicity analysis incorporating non-parametric methods. [Colour figure can be viewed at wileyonlinelibrary.com]

(Fig. 8J), and the phase-change histogram of the DR genes hints at phase shifts to a few hours earlier in the KO animals (Fig. 8K and L). Thirty-five genes were both differentially expressed and differentially regulated in a clock-dependent manner in the ROR α MKOs (Supplementary Table S2). Contrary to the PER2 MKOs, most genes are affected regardless of time of day, with 411 and 519 genes commonly upregulated or downregulated, respectively (Fig. 8M and N).

Commonly upregulated pathways are related to metabolism [respiratory electron transport, tricarboxylic acid (TCA) cycle, mitochondrial biogenesis, gluconeogenesis and amino acid metabolism] and the neuronal system (Fig. 9A) and are predicted to be regulated by the MYOG–MYOD1–RXRG and ESRRA transcription factor axes (Fig. 9B). Commonly downregulated pathways are related to skeletal muscle contractility (ion homeostasis, cardiac conduction, muscle contractions, stimuli-sensing channels and post-NMDA receptor activation events) and transport of small molecules (Fig. 9C), and the transcription factors MYF6, MEF2C, MEF2A and NR1D2 are predicted to be involved in their regulation (Fig. 9D). It is interesting to note that in the absence of ROR α , other nuclear receptors, such as RXRG (NR2B3), ESRRA and REV-ERBB (NR1D2), become more important for driving transcriptional responses in the muscle. The striking transcriptomic upregulation of genes encoding key mitochondrial enzymes in the ROR α MKO could explain the increased \dot{V}_{O_2} and energy expenditure observed in these mice (Fig. 4E and F, respectively) and also explains their improved exercise performance (Fig. 4B), independent of the time of day.

Looking into circadian-dependent changes in the transcriptome, the two time points that had the highest number of unique DR genes were ZT4 (rest phase) and ZT20 (active phase), with 323 and 361 upregulated genes (Fig. 8M) and 277 and 266 downregulated genes (Fig. 8N), respectively. Pathways relating to ERBB2 signalling, the immune system and triglyceride metabolism were uniquely upregulated at ZT4, whereas pathways related to muscle growth (extracellular matrix organization, PDGF signalling) and neuronal regulation (sensory perception, axon guidance, GPCR signalling) were uniquely upregulated at ZT20 (Fig. 9E). Metabolism of carbohydrates and ion homeostasis were uniquely downregulated at ZT4, whereas terms related to anti-

oxidant defence (amine oxidase reactions and glutathione synthesis and recycling) and nerve activity (NFAT activation, neuronal system) were downregulated at ZT20 (Fig. 9F). Our results could indicate a possible role of ROR α in regulating mitochondrial activity, metabolic regulation and glucose transport in the skeletal muscle, because its deletion leads to a compensatory increase of metabolic and mitochondrial genes.

Comparing the transcriptomic responses between the PER2 and ROR α MKOs, we see similarities in the terms that are significantly changed, but with circadian-dependent differences in their regulation. For example, the terms ‘metabolism’, ‘electron transport chain’, ‘TCA cycle’ and ‘RHO GTPase cycle’ are significantly upregulated at all ZTs in the ROR α MKOs, but are regulated in a circadian-dependent manner in the PER2 MKO, with the mitochondrial and metabolic terms being upregulated mostly at daytime (ZT0 and ZT4) and RHO GTPase cycle being upregulated at night-time (ZT12 and ZT16). Likewise, ‘amine oxidase reactions’ and ‘transport of small molecules’ are downregulated at most ZTs in the ROR α MKOs but specifically downregulated at ZT16 and ZT0, respectively, in PER2 MKOs. Some pathways are ubiquitously downregulated in both lines, such as ‘transport of amino acids/oligopeptides’ and ‘SLC-mediated membrane transport’, whereas others, such as ‘signal transduction’ is circadian specific for both (downregulated at ZT20 in ROR α MKOs and at ZT4 and ZT12 in PER2 MKOs).

Proteomic analysis of PER2 MKO muscle indicates a daytime specific role for PER2 in muscle metabolism and contraction

We next investigated the effects of PER2 ablation on protein levels by analysing the muscle proteome of sedentary mice harvested at ZT4 (resting period) and ZT16 (active/feeding period) by mass spectrometry.

Muscle-specific deletion of PER2 altered the expression level of 94 proteins at ZT4 (Fig. 10A and B) and 103 proteins at ZT16 (Fig. 10A and C), with an overlap of 23 proteins that were commonly altered at both time points (Fig. 10A). We then performed reactome pathway enrichment analysis of the up- and downregulated proteins at both time points. There were no statistically significant terms associated with the upregulated proteins in the inactive phase (ZT4), whereas in the active phase

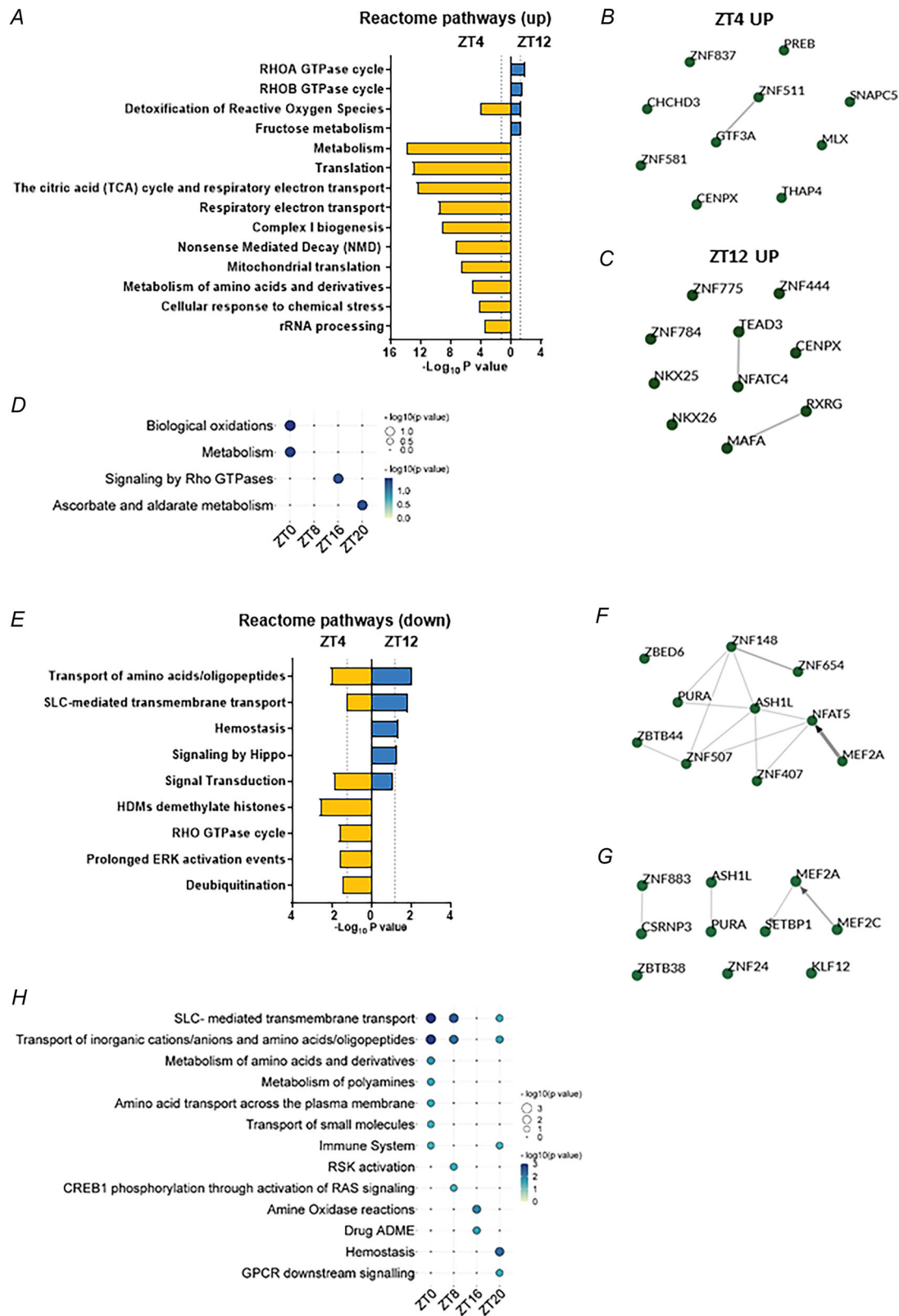


Figure 7. Pathway and transcription factor enrichment analysis of transcriptional responses to PER2 deletion at different time points

A, top 15 reactome pathways for upregulated differentially expressed genes (DEGs) in PER2 muscle-specific knockout (MKO) mice at zeitgeber time (ZT) 4 and ZT12. B and C, top 10 predicted transcription factors associated

with the upregulated DEGs at ZT4 (B) and ZT12 (C). D, dot plot of upregulated reactome pathways at ZT0, ZT8, ZT16 and ZT20. E, top 10 reactome pathways for differentially downregulated genes in PER2 MKO at ZT4 and ZT12. F and G, top 10 predicted transcription factors driving downregulated DEGs at ZT4 (F) and ZT12 (G). H, dot plot of downregulated reactome pathways at ZT0, ZT8, ZT16 and ZT20. Dashed lines indicate cut-off for significance at 1.3 ($P < 0.05$). [Colour figure can be viewed at wileyonlinelibrary.com]

(ZT16), proteins involved in ‘metabolism’, ‘metabolism of amino acids and derivatives’ and ‘urea cycle’ were significantly upregulated (Fig. 10D). On the contrary, many reactome pathways were downregulated at ZT4 (Fig. 10E), in particular, ‘muscle contraction’ and ‘striated muscle contraction’, while ‘metabolism’ and ‘amine oxidase reactions’ were commonly downregulated at both ZT4 and ZT16 (Fig. 10E). Proteins downregulated at ZT4 that contribute to the terms related to ‘muscle contraction’ include ATP2A2, ASPH, CAMK2D, DMD, DTNA, MYL2, MYLK2, TNNT1, TNNT3 and TNNT3, of which ASPH, DMD, DTNA and MYLK2 are also downregulated at ZT16. Proteins such as ME1, MAOB, PON3 and SMOX contribute to the terms ‘metabolism’ and ‘amine oxidase reactions’ and are commonly downregulated at ZT4 and ZT16. Interestingly, ‘metabolism of amino acids and derivatives’ is upregulated in the PER2 MKO at ZT16, but downregulated at ZT4 (Fig. 10D and E).

Comparing the transcriptomic and proteomic signatures in the MKOs, we observed that terms related to metabolism that were transcriptionally upregulated at ZT4 (Fig. 7A) translated to a proteomic upregulation of similar terms at ZT16 (Fig. 10D). This led us to look at the overlap between the differentially regulated proteins and genes at all time points. Almost half of all the proteins differentially regulated at either ZT4 or ZT16 were also differentially expressed transcriptomically (Fig. 10F and I), and most of these changes were driven by ZT4-specific changes in the transcriptome upon deletion of PER2 (Fig. 10G and J). Functionally, most of these overlapping proteins seem to be involved in the regulation of metabolism and amine oxidase reactions at both ZT4 and ZT16 (Fig. 10H and K), but could be regulated in opposing directions depending on the time of day, as is the case for metabolism of amino acids (Fig. 10D and E).

Proteomic analysis of ROR α MKO muscle indicates circadian-dependent and independent roles for ROR α in muscle metabolism and function

Muscle-specific deletion of ROR α affected the expression level of 196 proteins at ZT4 (Fig. 11A and B) and 412 proteins at ZT16 (Fig. 11A and C), with an overlap of 124 proteins that are commonly altered at both ZT4 and ZT16 (Fig. 11A).

Reactome pathway enrichment analysis indicated that the proteins upregulated in the ROR α MKO muscle

were largely involved in different pathways depending on the time of day. At ZT4, when the mice are inactive, proteins involved in ‘complex I biogenesis’, ‘respiratory electron transport’ and ‘TCA cycle’ were significantly upregulated (Fig. 11D). These terms mainly consisted of mitochondrial proteins, such as MT-CO2, MT-ND1, ME3, NDUFA1, NDUFA9, NDUFA13, NDUFAF6, NDUFC2, NDUFS2 and PDK1. At ZT16, when the mice are active, ‘rRNA processing’, ‘nonsense-mediated decay’, ‘translation initiation’, ‘metabolism of RNA’ and ‘neuronal system’ were significantly upregulated (Fig. 11D). The first four terms are mainly composed of ribosomal proteins (RPL10, RPL13A, RPL14, RPL18A, RPL19, RPL27, RPL8, RPS14, RPS18, RPS28, RPS3A1, RPS7 and WDR12) and AKT1, and the term ‘neuronal system’ consists of proteins such as ACTN2, GLUL, HOMER1, NEFL, KCNJ11 and KCNMA1. Proteins downregulated in the MKOs were both circadian-dependent and independent, with pathways related to ‘antigen presentation’, ‘post-translational protein phosphorylation’ and ‘regulation of IGF transport and uptake’ being commonly downregulated independent of the zeitgeber time (Fig. 11E). In contrast, pathways related to ‘amine oxidase reactions’, ‘detoxification of reactive oxygen species’ and ‘steroid metabolism’ were downregulated only at ZT16, while ‘muscle contraction’, ‘striated muscle contraction’ and ‘metabolism of amino acids and derivatives’ were downregulated specifically at ZT4 in ROR α MKOs (Fig. 11E). Proteins commonly downregulated at ZT4 and ZT16 that contribute to the terms ‘post-translational protein modification’ and ‘regulation of IGF transport and uptake’ are CALU, CST3, KTN1, LGALS1, P4HB and PRKCSH. Proteins downregulated at ZT4 that contribute to the terms related to ‘muscle contraction’ include ATP1A1, ATP2A1, ATP2A2, ASPH, CACNG6, CAMK2D, CASQ1, DMD, MYBPC2, MYL2, MYL3, TNNT1, TNNT1 and TNNT3, of which only ATP1A1, CASQ1 and DMD are also downregulated at ZT16.

It is interesting to note that although transcriptomic changes driven by deletion of ROR α were mostly circadian independent, the proteomic signature is specific for the time of day. For example, although mitochondrial activity (complex I biogenesis, TCA cycle and respiratory electron transport) and neuronal regulation were terms associated with commonly upregulated genes (Fig. 9A), they were specifically upregulated at ZT4 and ZT16, respectively, at the protein level (Fig. 11D). Likewise, muscle contraction, amino acid metabolism and NMDA receptor activation

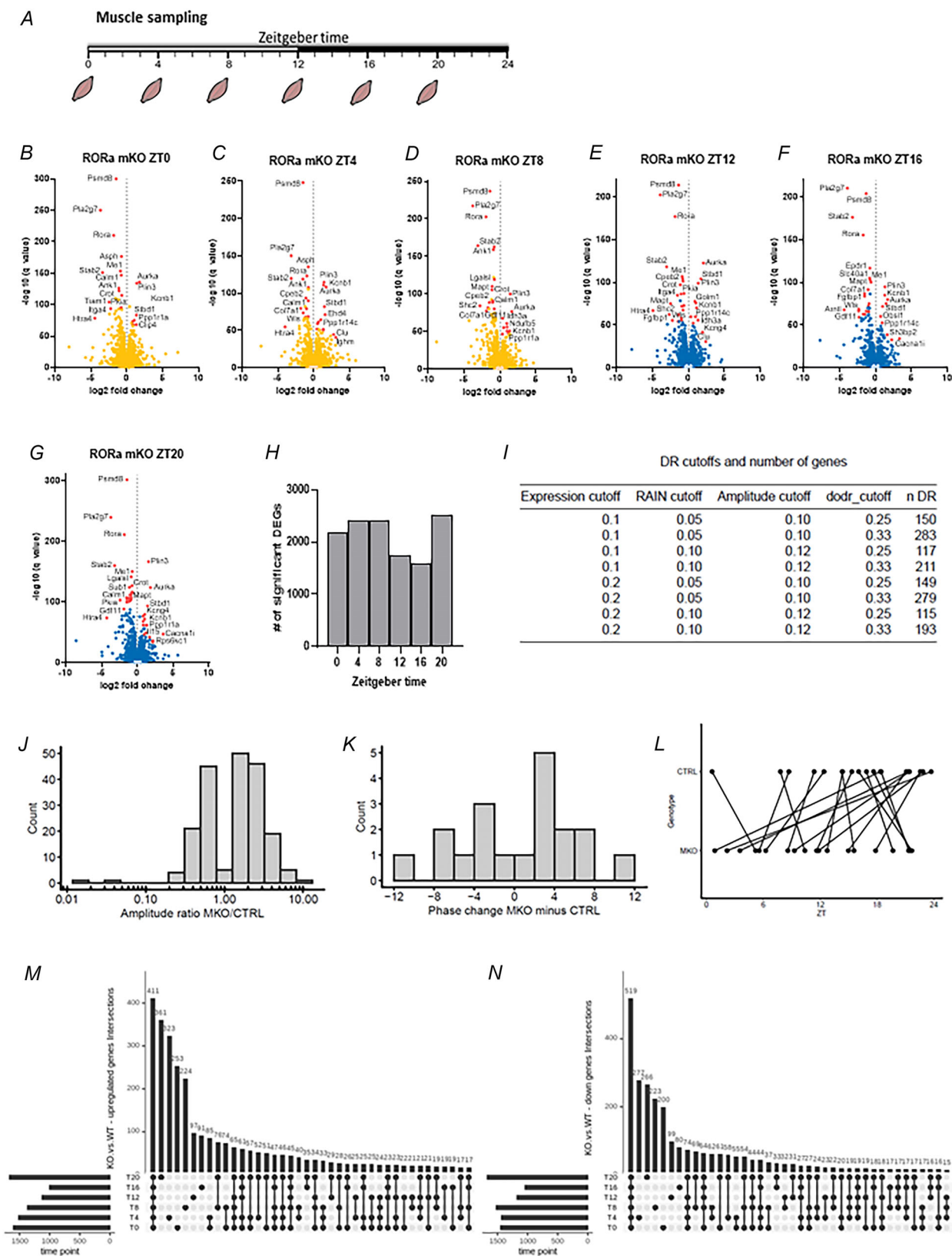


Figure 8. Time of day-specific transcriptional response to ROR α deletion in skeletal muscle
 A, schematic diagram of muscle sampling for RNA sequencing over 24 h. B–G, volcano plots displaying differentially expressed genes (DEGs) in ROR α muscle-specific knockout (MKO) mice relative to controls (CTRL) at zeitgeber

time (ZT) ZT0, ZT4, ZT8, ZT12, ZT16 and ZT20. The top 15 genes are labelled in red. *H*, number of significant DEGs (cut-off, $P < 0.05$) at each time point. *I*, table with summary of differentially regulated (DR) transcripts obtained with different statistical cut-offs. *J*, histogram distribution of amplitude fold change estimations of the 321 DR circadian transcripts in KO vs. CTRL mice. *K*, histogram of phase changes of DR genes in KO vs. CTRL mice. *L*, transcript phase shift analysis showing the shift of gene transcript expression at different times. *M* and *N*, upset plots showing overlaps between upregulated (*M*) and downregulated (*N*) DEGs at different time points. Abbreviations: DODR, detection of differential rhythmicity; RAIN, rhythmicity analysis incorporating non-parametric methods. [Colour figure can be viewed at wileyonlinelibrary.com]

were associated with commonly downregulated genes in the MKOs (Fig. 9C) but were specifically downregulated at ZT4 and ZT16 at the protein level (Fig. 11E). Comparing the overlap between the proteome and transcriptome, similar to the PER2 MKO, we observed that roughly half of all DR proteins at ZT4 and ZT16 were also DR transcriptomically (Fig. 11F and I). Only half of this overlap consists of genes that are commonly up- or downregulated at all ZTs in the absence of ROR α (Fig. 11G and J), implying that ROR α elicits both circadian-specific and broader changes in the muscle. For example, metabolism and regulation of amino acids are commonly altered at both ZT4 and ZT16 (Fig. 11H and K), whereas terms relating to mitochondrial activity, muscle contraction, neuronal activity and response to cellular stress are more specific for the time of day.

In addition, we also note similarities in how the two clock regulators affect the muscle, such as a shared downregulation of muscle contraction at ZT4 in both PER2 and ROR α MKOs (Fig. 10E and 11E). Pathways relating to metabolism, especially of polyamines and amino acids, in addition to amine oxidase reactions, are also altered in a similar manner when either feedback arm of the clock machinery is disrupted (Fig. 11L). However, there are also specific differences in both, such as upregulation of mitochondrial proteins and neuronal activity in the ROR α MKOs (Figs 9A and 11D), that could possibly be linked to improved treadmill performance (Fig. 4B).

Metabolomic analysis of PER2 and ROR α MKO muscle confirms dysregulation of amino acid metabolism

Given that dysregulation of amino acid and polyamine metabolism seemed to be one of most striking consequences of disrupting either feedback arm of the circadian clock, we performed metabolomic profiling of muscle tissues from the PER2 and ROR α MKOs at ZT4 (daytime) and ZT16 (night-time) to identify which metabolites were affected. In line with our transcriptomic and proteomic results, we could confirm that the top classes of metabolites that were differentially regulated in both MKOs were amino acids, amino acid-related metabolites and biogenic amines (Fig. 12, Supplementary Table S3). Both MKOs had significantly downregulated expression of amino acid and amine-related metabolites at ZT4, and downregulation of certain metabolites, such as carnosine and beta-alanine, also at ZT16 (Fig. 12A and B).

Glycine, proline, serine, threonine, valine, carnosine and beta-alanine were commonly downregulated in both MKOs, whereas other metabolites were more specific for either the PER2 or ROR α MKO. A complete list of all metabolites that were changed in both MKOs can be found in Supplementary Table S3. In general, the response to deletion of ROR α was more extensive, with a greater number and more significant downregulation of metabolites in the ROR α MKO compared with the PER2 MKO, consistent with the transcriptomic and proteomic signatures.

Discussion

The circadian clock and skeletal muscle function are tightly interlinked. The peripheral clock in skeletal muscle orchestrates a wide array of functions crucial for muscle health and performance. A network of clock genes and their downstream targets intricately control the regulation of energy metabolism, muscle contraction, exercise adaptations and myogenic processes. Disruptions to this clock machinery can lead to detrimental effects on muscle function and overall metabolic homeostasis. Exercise, a potent modulator of the skeletal muscle clock, has emerged as a promising candidate for entraining the circadian clock, thereby contributing to the prevention and treatment of individuals with metabolic diseases (Furrer et al., 2023; Gabriel & Zierath, 2019; Mansingh & Handschin, 2022; Xin et al., 2023). Recent works have extensively characterized the coordinated expression of the core clock factors BMAL1 and CLOCK within the muscle and identified their interaction with the muscle-specific transcription factor MYOD1 as a facilitator of the circadian and metabolic programmes that support skeletal muscle physiology (reviewed extensively by Martin et al., 2023b). However, there are various levels of feedback that regulate the temporal expression of the core clock loop, and muscle-specific regulation of factors, such as *Per2* and *Rora, which make up the primary and secondary arms of these feedback loops, have not been well characterized.*

In this study, therefore, we aimed to evaluate the functional and molecular consequences of modulating different regulatory loops of the muscle-intrinsic clock, through extensive phenotypic, transcriptomic, proteomic and metabolomic profiling of the muscle around the clock. Overall, deletion of PER2 and ROR α and, as a proxy,

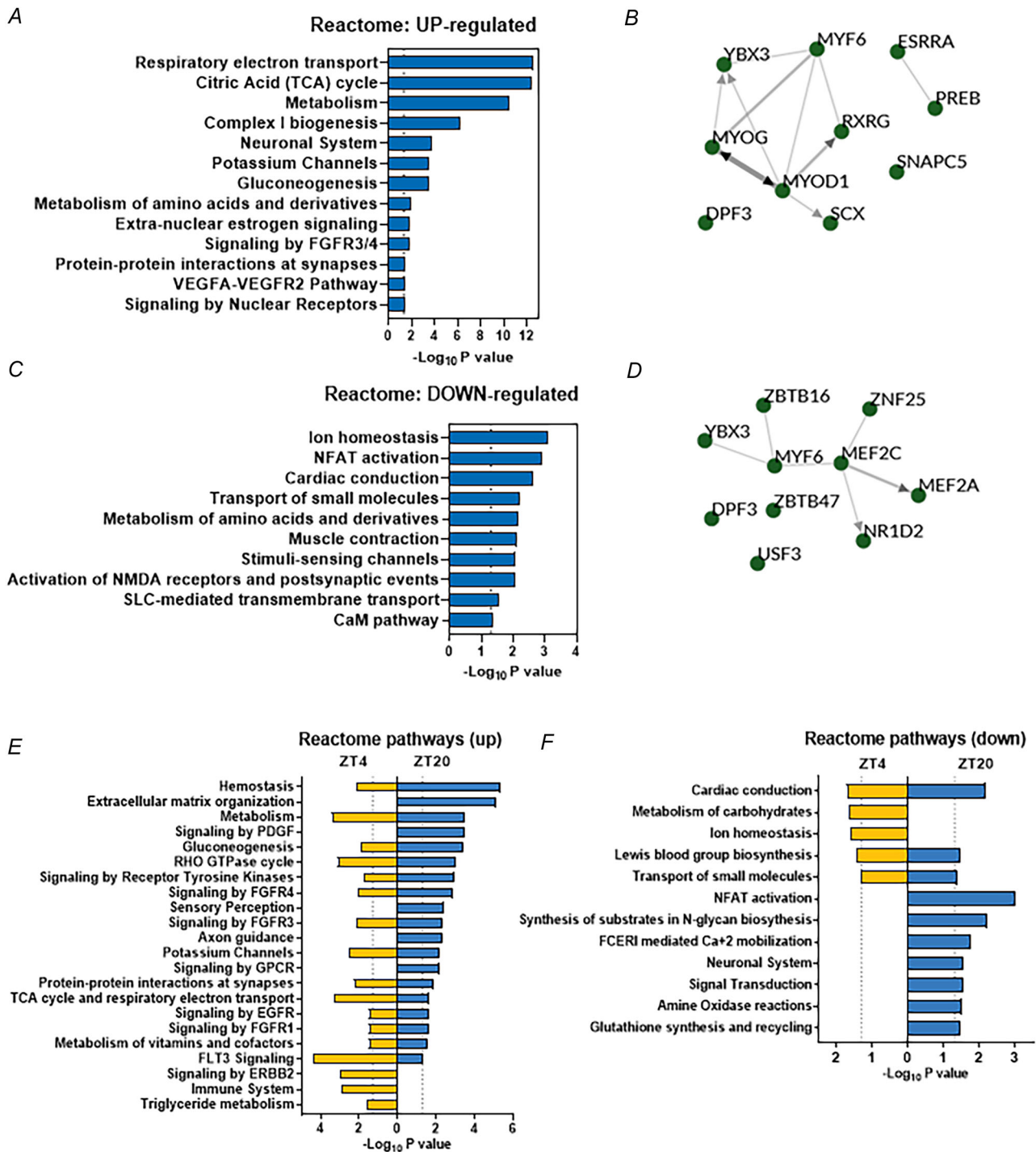


Figure 9. Transcriptional pathways and predicted transcription factor regulation in ROR α muscle-specific knockout mice

A, top reactome pathways for commonly upregulated differentially expressed genes (DEGs) in ROR α muscle-specific knockout (MKO) at all zeitgeber times (ZTs). B, top 10 predicted transcription factors driving upregulated DEGs. C, top reactome pathways for commonly downregulated DEGs in ROR α MKO at all ZTs. D, top 10 predicted transcription factors driving downregulated DEGs. E, top reactome pathways driving differentially upregulated genes in ROR α MKO at ZT4 and ZT20. F, top reactome pathways for differentially downregulated genes in ROR α MKO at ZT4 and ZT20. Dashed lines indicate cut-off for significance at 1.3 ($P < 0.05$). [Colour figure can be viewed at wileyonlinelibrary.com]

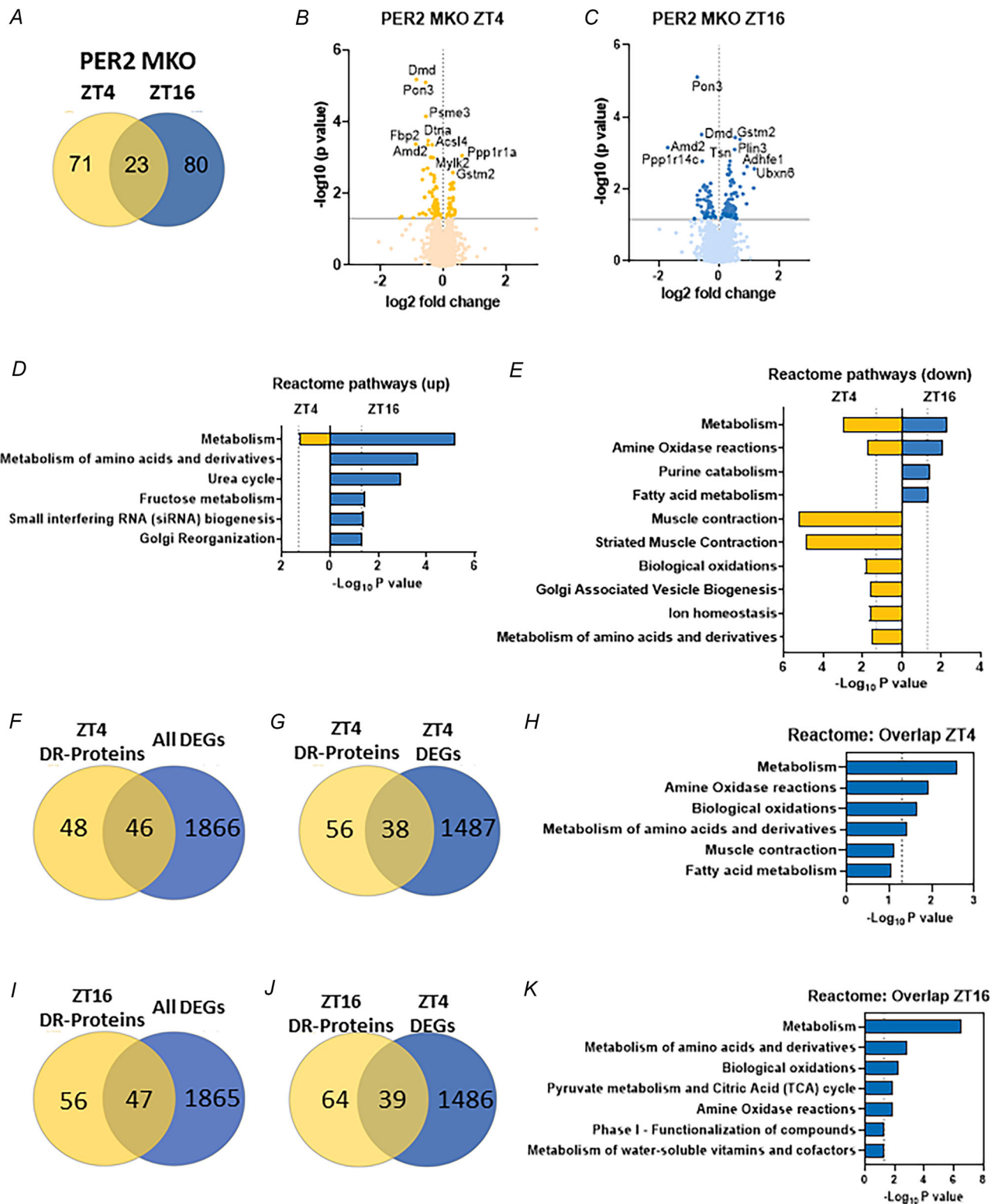


Figure 10. Proteomic analysis of PER2 muscle-specific knockout mice

A, Venn diagrams displaying the number of differentially expressed proteins in PER2 muscle-specific knockout (MKO) compared with control (CTRL) at daytime [zeitgeber time 4 (ZT4)] or night-time [zeitgeber time 16 (ZT16)] and resulting overlap. B and C, volcano plots displaying differentially regulated proteins (with top 10 indicated), as described above. D and E, reactome pathway enrichment analysis of upregulated (D) and downregulated (E) proteins in PER2 MKO mice at ZT4 and ZT16. F, overlap of all differentially regulated (DR) proteins at ZT4 with

differentially expressed genes (DEGs) at all time points in PER2 MKO. G, overlap of DR proteins with DEGs at ZT4. H, top reactome pathways for the 46 factors that overlap in F. I, overlap of all DR proteins at ZT16 with DEGs at all time points in PER2 MKO. J, overlap of DR proteins at ZT16 with DEGs at ZT4. K, top reactome pathways for the 47 factors that overlap in I. Grey and dashed lines indicate cut-off for significance at 1.3 ($P < 0.05$). [Colour figure can be viewed at wileyonlinelibrary.com]

modulation of the primary or secondary feedback arms, leads to shared, but also distinct outcomes in terms of transcriptome, proteome and phenotype.

First, perturbations of the primary (PER2 MKO) and secondary arms (ROR α MKO) of the core clock both dampen the amplitude of expression of many clock and clock-associated genes, but do not affect their phase, thereby maintaining basic circadian oscillation in the muscle. The reduction in amplitude of most clock genes is much stronger in the ROR α MKOs compared with the PER2 MKOs, which could be attributed to the opposing roles of ROR α and PER2 in activating and repressing the transcription of core clock genes, respectively. There might be more contingencies for perturbations in the primary loop than in the secondary loop, which could lead to compensatory effects from other isoforms in the case of the PER2 MKO, whereas in the ROR α MKO there could be less compensation in all aspects, not only the core clock. Additionally, given that the knockdown of ROR α also induces downregulation of *Bmal1* mRNA levels, it is possible that some of the effects we observed in the ROR α MKOs are mediated by the downregulation of *Bmal1*, which is supported by the parallels between the metabolic dysregulation observed in our model and those of BMAL1 MKOs (Dyar et al., 2018). These results reinforce the notion of high resilience of the muscle clock to phase shifts, e.g. similar to what has been observed in voluntary daytime running (Maier et al., 2022). Of note, subtle shifts in phase might be missed owing to the temporal resolution offered by a 4 h sampling time over 24 h. Nevertheless, the behaviour of the muscle clock in this regard is different from at least some other peripheral clocks, exemplified by the almost complete 12 h shift of the liver clock by daytime feeding (Damiola et al., 2000; Maier et al., 2022). Although exercise and physical activity should be promoted regardless of time of the day to increase compliance and adherence, circadian differences might arise from the more pliable molecular clocks in other organs, in particular those mediating substrate provisioning, such as the liver.

Second, arising from the transcriptomic, proteomic and metabolomics data, both knockouts, hence perturbation of both feedback loops, modulate genes encoding proteins involved in amino acid metabolism, urea cycle and amine oxidase activity, hence all linked to amine group homeostasis. This observation was substantiated in the metabolomic profiling that identified metabolites belonging to amino acid, amino acid-related and biogenic amine groups to be altered as a consequence of the deletion of PER2 and ROR α in the muscle. The

consequences of this alteration could be manifold, ranging from proteostasis to TCA cycle refuelling and hepatic gluconeogenesis. In the transcriptome, an upregulation of metabolic pathways, mostly centred on the TCA cycle, and a downregulation of SLC-mediated transmembrane transport are, likewise, commonly regulated pathways, although these seem to be more restricted for time of day in the PER2 MKOs compared with the ROR α MKOs. An inverse observation was made in terms of change in oscillation of non-clock genes, for which a much more substantial number was found in the PER2 MKOs. It is interesting to note that despite having fewer total genes changing in the PER2 MKOs, the changes observed in metabolic parameters were distinct, hinting at a more targeted role of PER2 in the muscle. However, we can comment only on parameters that we could observe, and it is possible that ROR α MKOs display other behavioural and metabolic changes that we could not elucidate with our present methods. Nevertheless, both factors seem to affect the rhythmicity of various muscle genes, even in the absence of a shift in the core clock gene expression. Finally, in addition to amino acid metabolism, an overlap in the proteome was found for downregulation of muscle contraction at ZT4, hinting at a circadian-dependent regulation of related functions.

Intriguingly, besides these commonalities, the ablation of ROR α and PER2 in skeletal muscle also leads to divergent outcomes. For example, the extent of perturbation is much larger for ROR α than for PER2, which could be interpreted as a more constricted involvement of the primary feedback loop in the core clock and a more loose function of the secondary arm. This is reflected in the higher number of circadian-dependent modulated genes and proteins in the PER2 MKOs compared with ROR α in the context of a higher total number of differentially regulated genes and proteins in the latter model. Alternatively, both PER2 and ROR α obviously could exert functions outside of the regulation of the clock, with ROR α doing this in a much broader manner than PER2. As a consequence, besides the differences in absolute numbers, a more time-restricted pattern was found for PER2 in as much as deletion of PER2 induces transcriptomic changes in the muscle specifically at ZT4 (peak daytime, resting/inactive phase), whereas the most transcriptomic changes observed upon the deletion of ROR α are independent of the time of day. Likewise, distinct pathways are implied by the non-overlapping changes in the proteome, e.g. for proteins related to mitochondrial activity and neuronal regulation that are unique to the ROR α MKOs.

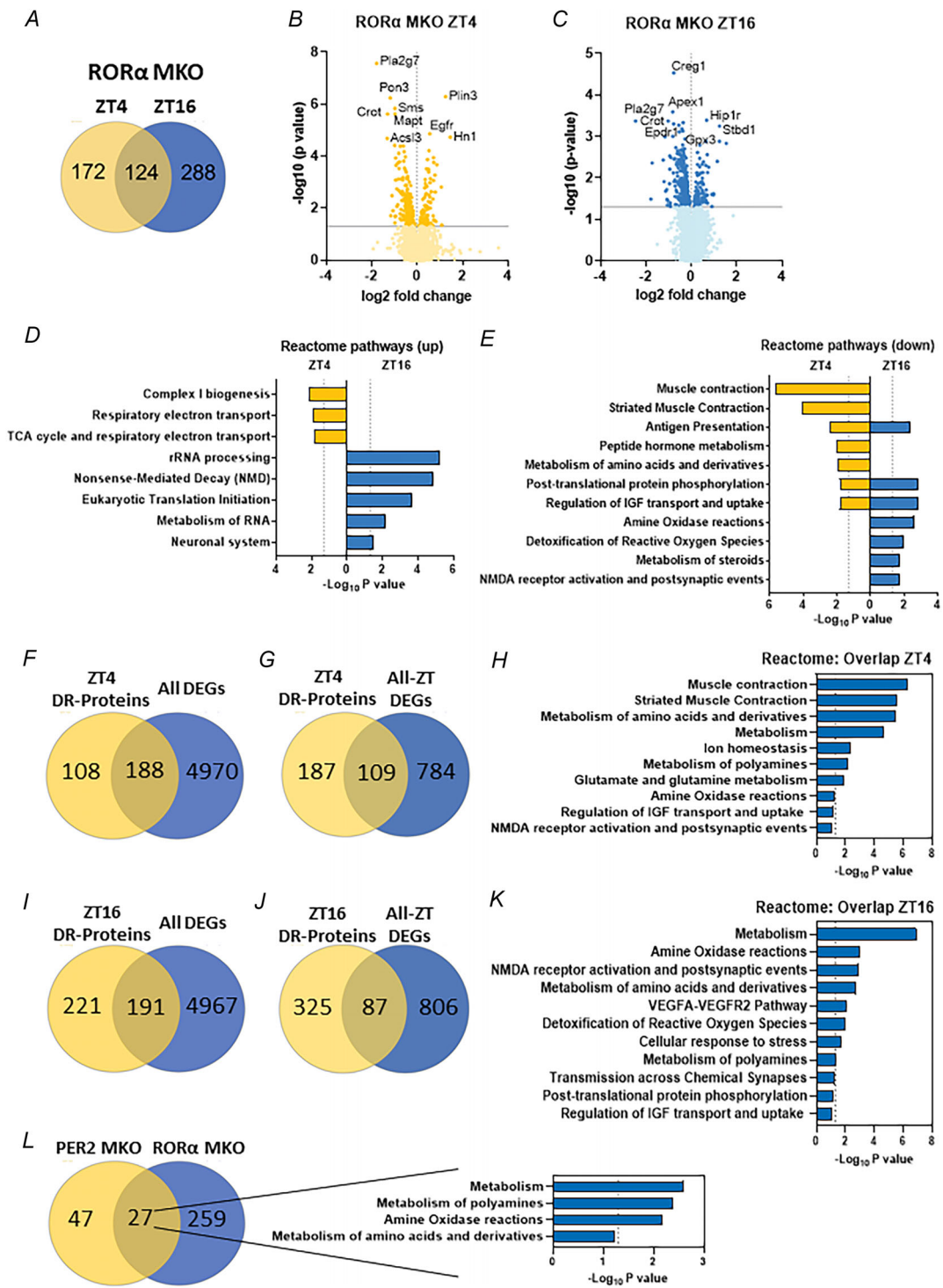


Figure 11. Proteomic analysis of ROR α muscle-specific knockout mice

A, Venn diagrams displaying the number of differentially expressed proteins in ROR α muscle-specific knockout (MKO) compared with control (CTRL) at daytime [zeitgeber time 4 (ZT4)] or night-time [zeitgeber time 16 (ZT16)] and resulting overlap. B and C, volcano plots displaying differentially regulated (DR) proteins (with the top 10 indicated), as described above. D and E, reactome pathway enrichment analysis of upregulated (D) and down-regulated (E) proteins in ROR α MKO mice at ZT4 and ZT16. F, overlap of all DR proteins at ZT4 with differentially expressed genes (DEGs) at all time points in ROR α MKO. G, overlap of DR proteins with genes commonly DR at all ZTs. H, top reactome pathways for the 188 factors that overlap in F. I, overlap of all DR proteins at ZT16 with DEGs at all time points in ROR α MKO. J, overlap of DR proteins at ZT16 with genes commonly DR at all ZTs. K,

top reactome pathways for the 191 factors that overlap in *I. L.*, overlap between genes and proteins that were commonly different in PER2 and ROR α MKO at all time points. Top reactome pathways associated with the 27 overlapping factors are depicted within the black lines. Grey and dashed lines indicate cut-off for significance at 1.3 ($P < 0.05$). [Colour figure can be viewed at wileyonlinelibrary.com]

The findings of the transcriptomic and proteomic analysis are reflected at the physiological level. We observed diurnal changes in glucose metabolism, with both MKOs showing reduced glucose tolerance during the daytime (resting/inactive phase), which returned to

baseline at night (feeding/active phase) in the PER2 MKO and improved even further in the ROR α MKO. Feeding patterns and body composition remained unaltered in both MKOs, whereas activity level (and subsequent core body temperature) was distinctly affected in PER2 MKOs,

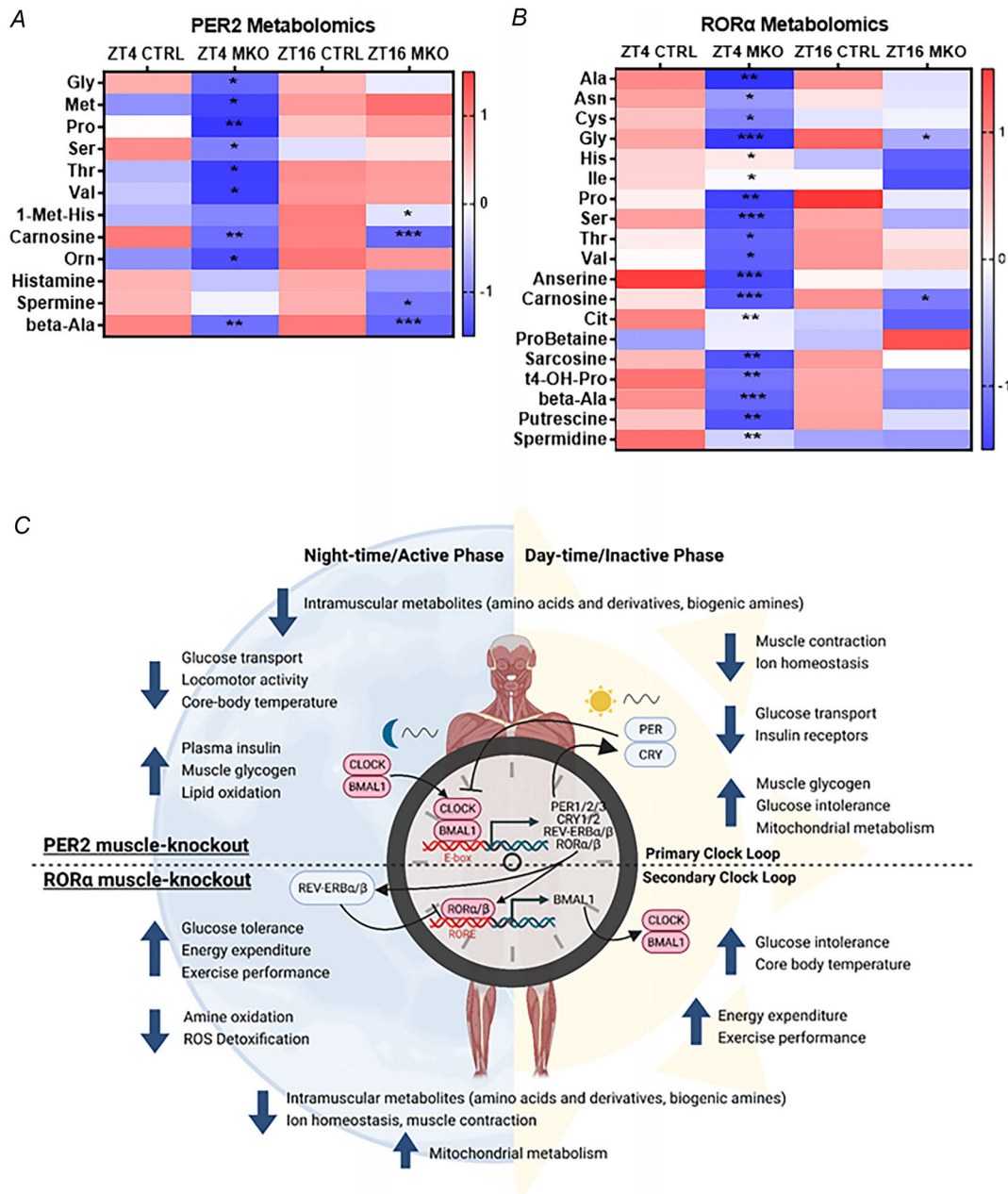


Figure 12. Metabolomic analysis of PER2 and ROR α muscle-specific knockout mice

A, heatmap displaying metabolites that are significantly differentially regulated in the PER2 muscle-specific knockout (MKO) at zeitgeber time 4 (ZT4) or zeitgeber time 16 (ZT16). B, heatmap displaying metabolites that

are significantly differentially regulated in the ROR α MKOs compared with control at daytime (ZT4) or night-time (ZT16). Data shown are averaged z-score values of five or six animals (n) per genotype per time point. * $q < 0.05$, ** $q < 0.01$ and *** $q < 0.001$; Student's unpaired t test. C, schematic diagram depicting the primary and secondary molecular clock loops, with a summary of all the main results from this study. Please note that the study was conducted entirely in mice and the human figure is for illustrative purposes. This figure was created with BioRender.com. Abbreviations: Ala, alanine; Asn, asparagine; Cit, citrullin; Cys, cysteine; Gly, glycine; His, histidine; Ile, isoleucine; Met, methionine; Orn, ornithine; Pro, proline; Ser, serine; Thr, threonine; Val, valine. [Colour figure can be viewed at wileyonlinelibrary.com]

with lower voluntary night-time locomotor activity and body temperature but with no effect on exercise capacity when forced. In contrast, although general activity levels were unaffected in ROR α MKOs, they showed an improved capacity to exercise when challenged, independent of the time of day. They also displayed a circadian-independent increase in energy expenditure and oxygen consumption, with no changes in substrate preference, despite a moderate shift in fibre-type distribution towards type IIx fibres.

It is important to note here that in mice, activity during day and night is opposite to that in humans. Hence, for human translational aspects, the results discussed so far would have to be mirrored for the light and dark phase, especially when it comes to activity and feeding status. Our preclinical findings in mice are corroborated by recent studies in humans, in which reduced 24 h variations in RER, higher glucose levels and increased triglyceride levels were observed in older, metabolically compromised humans compared with healthy young control subjects, and this metabolic inflexibility was associated with altered PER2 rhythmicity in the skeletal muscle (Wefers et al., 2020). Various studies have shown that mitochondrial dynamics are under circadian control and that changes in rhythmicity of mitochondrial genes are closely related to the development of insulin resistance and type 2 diabetes (Gabriel et al., 2021; Hansen et al., 2016; van Moorsel et al., 2016). Our data point towards a similar mechanism of action in the PER2 and ROR α MKOs, confirming that perturbation of the circadian feedback loops leads to alterations in the bidirectional communication between mitochondrial function and rhythmic gene expression. The potentially prediabetic phenotype observed in our mouse models could be a consequence of this impairment, which has also been shown to be correlated with the development of diabetes in human studies (Gabriel et al., 2021; van Moorsel et al., 2016; Wefers et al., 2020).

In conclusion, the different feedback loops of the core clock affect a few common properties, but also very distinct genes, proteins and pathways, leading to divergent phenotypic outcomes. The specific reciprocal regulation of clock (primary/secondary feedback arm) and the muscle activity–exercise–inactivity axis might thus be crucial to determine specific outcomes for muscle plasticity. Our comprehensive transcriptome, proteome and metabolome analyses might provide a starting point to dissect out specific pathways that could be targeted

to rescue impairments in desynchronization between the central and muscle-intrinsic clocks. In addition, future work dissecting out the consequences of timed exercise or restricted feeding on regulation of the muscle plasticity in the absence of PER2 or ROR α would also be valuable in paving the way for potential therapeutic applications to enhance muscle function and mitigate associated disorders.

References

- Ahrné, E., Glatter, T., Viganò, C., von Schubert, C., Nigg, E. A., & Schmidt, A. (2016). Evaluation and improvement of quantification accuracy in isobaric mass tag-based protein quantification experiments. *Journal of Proteome Research*, *15*(8), 2537–2547.
- Andrews, J. L., Zhang, X., McCarthy, J. J., McDearmon, E. L., Hornberger, T. A., Russell, B., Campbell, K. S., Arbogast, S., Reid, M. B., Walker, J. R., Hogenesch, J. B., Takahashi, J. S., & Esser, K. A. (2010). CLOCK and BMAL1 regulate *MyoD* and are necessary for maintenance of skeletal muscle phenotype and function. *Proceedings of the National Academy of Sciences of the United States of America*, *107*(44), 19090–19095.
- Bae, K., Jin, X., Maywood, E. S., Hastings, M. H., Reppert, S. M., & Weaver, D. R. (2001). Differential functions of mPer1, mPer2, and mPer3 in the SCN circadian clock. *Neuron*, *30*(2), 525–536.
- Bae, K., Lee, K., Seo, Y., Lee, H., Kim, D., & Choi, I. (2006). Differential effects of two period genes on the physiology and proteomic profiles of mouse anterior tibialis muscles. *Molecules and Cells*, *22*(3), 275–284.
- Bass, J., & Lazar, M. A. (2016). Circadian time signatures of fitness and disease. *Science*, *354*(6315), 994–999.
- Bass, J., & Takahashi, J. S. (2010). Circadian integration of metabolism and energetics. *Science*, *330*(6009), 1349–1354.
- Billon, C., Sitaula, S., & Burris, T. P. (2017). Metabolic characterization of a novel ROR α knockout mouse model without Ataxia. *Frontiers in Endocrinology*, *8*, 141.
- Bolger, A. M., Lohse, M., & Usadel, B. (2014). Trimmomatic: A flexible trimmer for Illumina sequence data. *Bioinformatics*, *30*(15), 2114–2120.
- Chavan, R., Feillet, C., Costa, S. S. F., Delorme, J. E., Okabe, T., Ripperger, J. A., & Albrecht, U. (2016). Liver-derived ketone bodies are necessary for food anticipation. *Nature Communications*, *7*(1), 10580.
- Conway, J. R., Lex, A., & Gehlenborg, N. (2017). UpSetR: An R package for the visualization of intersecting sets and their properties. *Bioinformatics*, *33*(18), 2938–2940.

- Damiola, F., Le Minh, N., Preitner, N., Kornmann, B., Fleury-Olela, F., & Schibler, U. (2000). Restricted feeding uncouples circadian oscillators in peripheral tissues from the central pacemaker in the suprachiasmatic nucleus. *Genes & Development*, **14**(23), 2950–2961.
- Delezie, J., Dumont, S., Dardente, H., Oudart, H., Gréchez-Cassiau, A., Klosen, P., Teboul, M., Delaunay, F., Pévet, P., & Challet, E. (2012). The nuclear receptor REV-ERB α is required for the daily balance of carbohydrate and lipid metabolism. *The Federation of American Societies of Experimental Biology Journal*, **26**(8), 3321–3335.
- Dibner, C., Schibler, U., & Albrecht, U. (2010). The mammalian circadian timing system: Organization and coordination of central and peripheral clocks. *Annual Review of Physiology*, **72**(1), 517–549.
- Dobin, A., Davis, C. A., Schlesinger, F., Drenkow, J., Zaleski, C., Jha, S., Batut, P., Chaisson, M., & Gingeras, T. R. (2013). STAR: Ultrafast universal RNA-seq aligner. *Bioinformatics (Oxford, England)*, **29**(1), 15–21.
- Dyar, K. A., Ciciliot, S., Wright, L. E., Biensø, R. S., Tagliazucchi, G. M., Patel, V. R., Forcato, M., Paz, M. I. P., Gudiksen, A., Solagna, F., Albiro, M., Moretti, I., Eckel-Mahan, K. L., Baldi, P., Sassone-Corsi, P., Rizzuto, R., Bicciato, S., Pilegaard, H., Blaauw, B., & Schiaffino, S. (2014). Muscle insulin sensitivity and glucose metabolism are controlled by the intrinsic muscle clock. *Molecular Metabolism*, **3**(1), 29–41.
- Dyar, K. A., Hubert, M. J., Mir, A. A., Ciciliot, S., Lutter, D., Greulich, F., Quagliarini, F., Kleinert, M., Fischer, K., Eichmann, T. O., Wright, L. E., Peña Paz, M. I., Casarin, A., Pertegato, V., Romanello, V., Albiro, M., Mazzucco, S., Rizzuto, R., Salviati, L., ... Uhlenhaut, N. H. (2018). Transcriptional programming of lipid and amino acid metabolism by the skeletal muscle circadian clock. *PLoS Biology*, **16**(8), e2005886.
- Eckel-Mahan, K., & Sassone-Corsi, P. (2013). Metabolism and the circadian clock converge. *Physiological Reviews*, **93**(1), 107–135.
- Ewels, P., Magnusson, M., Lundin, S., & Käller, M. (2016). MultiQC: Summarize analysis results for multiple tools and samples in a single report. *Bioinformatics*, **32**(19), 3047–3048.
- Furrer, R., Hawley, J. A., & Handschin, C. (2023). The molecular athlete: Exercise physiology from mechanisms to medals. *Physiological Reviews*, **103**(3), 1693–1787.
- Gabriel, B. M., Altıntaş, A., Smith, J. A. B., Sardon-Puig, L., Zhang, X., Basse, A. L., Laker, R. C., Gao, H., Liu, Z., Dollet, L., Treebak, J. T., Zorzano, A., Huo, Z., Rydén, M., Lanner, J. T., Esser, K. A., Barrès, R., Pilon, N. J., Krook, A., & Zierath, J. R. (2021). Disrupted circadian oscillations in type 2 diabetes are linked to altered rhythmic mitochondrial metabolism in skeletal muscle. *Science Advances*, **7**(43), eabi9654.
- Gabriel, B. M., & Zierath, J. R. (2019). Circadian rhythms and exercise — re-setting the clock in metabolic disease. *Nature Reviews Endocrinology*, **15**(4), 197–206.
- Gutierrez-Monreal, M. A., Harmsen, J., Schrauwen, P., & Esser, K. A. (2020). Ticking for metabolic health: The skeletal-muscle clocks. *Obesity*, **28**(S1), S46–S54.
- Hansen, J., Timmers, S., Moonen-Kornips, E., Duez, H., Staels, B., Hesselink, M. K. C., & Schrauwen, P. (2016). Synchronized human skeletal myotubes of lean, obese and type 2 diabetic patients maintain circadian oscillation of clock genes. *Scientific Reports*, **6**(1), 35047.
- Harfmann, B. D., Schroder, E. A., Kachman, M. T., Hodge, B. A., Zhang, X., & Esser, K. A. (2016). Muscle-specific loss of Bmal1 leads to disrupted tissue glucose metabolism and systemic glucose homeostasis. *Skeletal Muscle*, **6**(1), 12.
- Huang, D. W., Sherman, B. T., & Lempicki, R. A. (2009). Systematic and integrative analysis of large gene lists using DAVID bioinformatics resources. *Nature Protocols*, **4**(1), 44–57.
- Katoku-Kikyo, N., Paatela, E., Houtz, D. L., Lee, B., Munson, D., Wang, X., Hussein, M., Bhatia, J., Lim, S., Yuan, C., Asakura, Y., Asakura, A., & Kikyo, N. (2021). Per1/Per2–Igf2 axis-mediated circadian regulation of myogenic differentiation. *Journal of Cell Biology*, **220**(7), e202101057.
- Keenan, A. B., Torre, D., Lachmann, A., Leong, A. K., Wojciechowicz, M. L., Utti, V., Jagodnik, K. M., Kropiwnicki, E., Wang, Z., & Ma'ayan, A. (2019). ChEA3: Transcription factor enrichment analysis by orthogonal omics integration. *Nucleic Acids Research*, **47**(W1), W212–W224.
- Lau, P., Fitzsimmons, R. L., Pearen, M. A., Watt, M. J., & Muscat, G. E. O. (2011). Homozygous staggerer (sg/sg) mice display improved insulin sensitivity and enhanced glucose uptake in skeletal muscle. *Diabetologia*, **54**(5), 1169–1180.
- Love, M. I., Huber, W., & Anders, S. (2014). Moderated estimation of fold change and dispersion for RNA-seq data with DESeq2. *Genome Biology*, **15**(12), 550.
- Maier, G., Delezie, J., Westermarck, P. O., Santos, G., Ritz, D., & Handschin, C. (2022). Transcriptomic, proteomic and phosphoproteomic underpinnings of daily exercise performance and zeitgeber activity of training in mouse muscle. *The Journal of Physiology*, **600**(4), 769–796.
- Mansingh, S., & Handschin, C. (2022). Time to train: The involvement of the molecular clock in exercise adaptation of skeletal muscle. *Frontiers in Physiology*, **13**, 902031.
- Marcheva, B., Ramsey, K. M., Buhr, E. D., Kobayashi, Y., Su, H., Ko, C. H., Ivanova, G., Omura, C., Mo, S., Vitaterna, M. H., Lopez, J. P., Philipson, L. H., Bradfield, C. A., Crosby, S. D., JeBailey, L., Wang, X., Takahashi, J. S., & Bass, J. (2010). Disruption of the clock components CLOCK and BMAL1 leads to hypoinsulinaemia and diabetes. *Nature*, **466**(7306), 627–631.
- Martin, R. A., Viggars, M. R., & Esser, K. A. (2023a). Metabolism and exercise: The skeletal muscle clock takes centre stage. *Nature Reviews Endocrinology*, **19**(5), 272–284.
- Martin, R. A., Viggars, M. R., & Esser, K. A. (2023b). Metabolism and exercise: The skeletal muscle clock takes centre stage. *Nature Reviews Endocrinology*, **19**(5), 272–284.
- Partch, C. L., Green, C. B., & Takahashi, J. S. (2014). Molecular architecture of the mammalian circadian clock. *Trends in Cell Biology*, **24**(2), 90–99.

- Peek, C. B., Levine, D. C., Cedernaes, J., Taguchi, A., Kobayashi, Y., Tsai, S. J., Bonar, N. A., McNulty, M. R., Ramsey, K. M., & Bass, J. (2017). Circadian clock interaction with HIF1 α mediates oxygenic metabolism and anaerobic glycolysis in skeletal muscle. *Cell Metabolism*, **25**(1), 86–92.
- Pendergast, J. S., Friday, R. C., & Yamazaki, S. (2010). Distinct functions of Period2 and Period3 in the mouse circadian system revealed by in vitro analysis. *PLoS ONE*, **5**(1), e8552.
- Perrin, L., Loizides-Mangold, U., Chanon, S., Gobet, C., Hulo, N., Isenegger, L., Weger, B. D., Migliavacca, E., Charpagne, A., Betts, J. A., Walhin, J.-P., Templeman, I., Stokes, K., Thompson, D., Tsintzas, K., Robert, M., Howald, C., Riezman, H., Feige, J. N., ... Dibner, C. (2018). Transcriptomic analyses reveal rhythmic and CLOCK-driven pathways in human skeletal muscle. *Elife*, **7**, e34114.
- Raichur, S., Fitzsimmons, R. L., Myers, S. A., Pearen, M. A., Lau, P., Eriksson, N., Wang, S. M., & Muscat, G. E. O. (2010). Identification and validation of the pathways and functions regulated by the orphan nuclear receptor, ROR alpha1, in skeletal muscle. *Nucleic Acids Research*, **38**(13), 4296–4312.
- Schmutz, I., Ripperger, J. A., Baeriswyl-Aebischer, S., & Albrecht, U. (2010). The mammalian clock component PERIOD2 coordinates circadian output by interaction with nuclear receptors. *Genes & Development*, **24**(4), 345–357.
- Sherman, B. T., Hao, M., Qiu, J., Jiao, X., Baseler, M. W., Lane, H. C., Imamichi, T., & Chang, W. (2022). DAVID: A web server for functional enrichment analysis and functional annotation of gene lists (2021 update). *Nucleic Acids Research*, **50**(W1), W216–W221.
- Steinmayr, M., André, E., Conquet, F., Rondi-Reig, L., Delhaye-Bouchaud, N., Auclair, N., Daniel, H., Crépel, F., Mariani, J., Sotelo, C., & Becker-André, M. (1998). *staggerer* phenotype in retinoid-related orphan receptor α -deficient mice. *Proceedings of the National Academy of Sciences of the United States of America*, **95**(7), 3960–3965.
- Takahashi, J. S. (2017). Transcriptional architecture of the mammalian circadian clock. *Nature Reviews Genetics*, **18**(3), 164–179.
- Takahashi, J. S., Hong, H.-K., Ko, C. H., & McDearmon, E. L. (2008). The genetics of mammalian circadian order and disorder: Implications for physiology and disease. *Nature Reviews Genetics*, **9**(10), 764–775.
- Thaben, P. F., & Westermark, P. O. (2016). Differential rhythmicity: Detecting altered rhythmicity in biological data. *Bioinformatics*, **32**(18), 2800–2808.
- van Moorsel, D., Hansen, J., Havekes, B., Scheer, F. A. J. L., Jörgensen, J. A., Hoeks, J., Schrauwen-Hinderling, V. B., Duez, H., Lefebvre, P., Schaper, N. C., Hesselink, M. K. C., Staels, B., & Schrauwen, P. (2016). Demonstration of a day-night rhythm in human skeletal muscle oxidative capacity. *Molecular Metabolism*, **5**(8), 635–645.
- Wang, Y., Yang, F., Gritsenko, M. A., Wang, Y., Clauss, T., Liu, T., Shen, Y., Monroe, M. E., Lopez-Ferrer, D., Reno, T., Moore, R. J., Klemke, R. L., Camp, D. G., & Smith, R. D. (2011). Reversed-phase chromatography with multiple fraction concatenation strategy for proteome profiling of human MCF10A cells. *PROTEOMICS*, **11**(10), 2019–2026. Portico.
- Wefers, J., Connell, N. J., Fealy, C. E., Andriessen, C., de Wit, V., van Moorsel, D., Moonen-Kornips, E., Jörgensen, J. A., Hesselink, M. K. C., Havekes, B., Hoeks, J., & Schrauwen, P. (2020). Day-night rhythm of skeletal muscle metabolism is disturbed in older, metabolically compromised individuals. *Molecular Metabolism*, **41**, 101050.
- Xin, H., Huang, R., Zhou, M., Chen, J., Zhang, J., Zhou, T., Ji, S., Liu, X., Tian, H., Lam, S. M., Bao, X., Li, L., Tong, S., Deng, F., Shui, G., Zhang, Z., Wong, C. C. L., & Li, M.-D. (2023). Daytime-restricted feeding enhances running endurance without prior exercise in mice. *Nature Metabolism*, **5**(7), 1236–1251.
- Zambon, A. C., McDearmon, E. L., Salomonis, N., Vranizan, K. M., Johansen, K. L., Adey, D., Takahashi, J. S., Schambelan, M., & Conklin, B. R. (2003). Time- and exercise-dependent gene regulation in human skeletal muscle. *Genome Biology*, **4**(10), R61.
- Zani, F., Breasson, L., Becattini, B., Vukolic, A., Montani, J.-P., Albrecht, U., Provenzani, A., Ripperger, J. A., & Solinas, G. (2013). PER2 promotes glucose storage to liver glycogen during feeding and acute fasting by inducing *Gys2* PTG and GL expression. *Molecular Metabolism*, **2**(3), 292–305.
- Zhao, Y., Zhang, Y., Zhou, M., Wang, S., Hua, Z., & Zhang, J. (2012). Loss of *mPer2* increases plasma insulin levels by enhanced glucose-stimulated insulin secretion and impaired insulin clearance in mice. *FEBS Letters*, **586**(9), 1306–1311.
- Zheng, B., Albrecht, U., Kaasik, K., Sage, M., Lu, W., Vaishnav, S., Li, Q., Sun, Z. S., Eichele, G., Bradley, A., & Lee, C. C. (2001). Nonredundant roles of the *mPer1* and *mPer2* genes in the mammalian circadian clock. *Cell*, **105**(5), 683–694.

Additional information

Data availability statement

Transcriptomic data have been deposited at the Gene Expression Omnibus (GEO; accession number GSE243522). Proteomic data have been deposited at the Proteomics Identifications Database (MassIVE; accession number MSV000092804). Metabolomics data are available as an Excel file in the Supporting Information.

Competing interests

None declared.

Author contributions

Conceptualization: J.D., G.M. and C.H. Methodology: S.M., G.M., J.D., D.R., U.A. and C.H. Investigation: S.M., G.M., J.D., G.S., B.K.C. and S.A.S. Formal analysis and visualization: S.M., G.M., W.D., P.O.W. and D.R. Writing: S.M. and C.H. Funding acquisition: C.H. All authors have read and approved the final version of this manuscript and agree to be accountable for all aspects of the work in ensuring that questions related to the accuracy or integrity of any part of the work are appropriately investigated and resolved. All persons designated as authors qualify for authorship, and all those who qualify for authorship are listed.

Funding

This research was supported by grants from the Swiss National Science Foundation (SNSF; grant 310 030_184 832 and grant CRSII5_209 252), the Swiss Society for Research on Muscle Diseases (SSEM), the Jain Foundation, the Novartis Stiftung für Medizinisch-Biologische Forschung, the Biozentrum PhD Fellowship Program and the University of Basel.

Acknowledgements

We thank the Quantitative Genomics Facility of the University of Basel, in particular Phillippe Demougin, for preparing cDNA libraries. Calculations were performed at sciCORE (<http://scicore.unibas.ch/>) scientific computing centre at University of Basel, with support by the Swiss Institute of Bioinformatics (SIB).

Open access funding provided by Universitat Basel.

Keywords

circadian rhythm, exercise, metabolism, molecular clock, PER2, ROR α , skeletal muscle, transcriptional regulation

Supporting information

Additional supporting information can be found online in the Supporting Information section at the end of the HTML view of the article. Supporting information files available:

Peer Review History

Supplementary Table 1

Supplementary Table 2

Supplementary Table 3